Determination of the energy landscape among biological macromolecules: The mucin-alginate case

Patricia Safaee Adl

Norwegian University of Science and Technology
Department of Physics

Norwegian University of Science and Technology

Master's Thesis

***Determination of the energy landscape among biological macromolecules:
The mucin-alginate case***

Author:
Patricia Safaee Adl

Supervisor:
Bjørn Torger Stokke

June 17th, 2013

Abstract

Luminal epithelial surfaces of our body are covered by a secreted layer of mucus consisting chiefly of water (95%), high molecular weight polymeric glycoproteins known as mucins (3%), and other small molecules (2%). If this layer infected by bacterial alginate it will cause the mucus being sticky.

Cystic fibrosis is a complex, incurable, chronic, hereditary disease involving several body organs systems, which affects the body glands that produce mucus and sweat. Although multiple microbial species can colonize the CF lung, CF patients are particularly have infected by an alginate secreting bacteria, which is called *Pseudomonas Aeruginosa*, it can be one of the major cause of decline in lung function and death.

Alginate can significantly increase the elasticity and viscosity of the mucus. Alginates are relatively abundant in nature because they arise both as a structural component in marine brown algae (*Phaeophyceae*), comprising up to 40% of the dry matter, and as capsular polysaccharides in soil bacteria. Alginates are naturally occurring polysaccharides synthesized in brown algae and certain types of bacteria and have been extensively used as hydrogel synthetic ECMs.

In this study interactions of different concentration of Mucin and different alginates are considered, their force jumps of single molecule interactions collected and analysed by Lifetime analysis and Bell Evans analysis.

Presence of Ca^{2+} and its significant influence on mucin-alginate bonds are studied as well.

IV

Acknowledgments

This master thesis would not have been possible without the support of many people. I wish to express my gratitude to my supervisor, Prof. Dr. Bjørn Torger Stokke who was abundantly helpful and offered priceless assistance, support and guidance. I would also like to convey a special thank Gjertrud Maurstad because of her endless help.

Special thanks also to all my graduate friends, especially group member, Armend Håti for sharing the literature and invaluable assistance, without his knowledge and assistance this study would not have been successful.

I would like to take this opportunity to thank my beloved Masoud, who has helped me by his patience, love and endless support.

I wish to express my love and gratitude to the true roses of my life, my mother and father; who have always stimulated me to stay open-minded and to keep on doing the best I could, and thank them for their understanding & endless love, through the duration of my studies.

Table of Contents

1. Introduction

1.1 Cystic Fibrosis

Cystic fibrosis is a complex, incurable, chronic, hereditary disease involving several body organs systems, which affects the body glands that produce mucus and sweat. [1] Cystic fibrosis is caused by mutations in the gene, which is responsible for the CF transmembrane conductance regulator (CFTR), which is a membrane glycoprotein that is contributing in regulation of ion flux at certain epithelial surfaces. [2] A defective gene and its protein product cause the body mucus to become thick and sticky when mucus builds up, it can unfortunately block the airways of the lungs and meanwhile encourages the growth of bacteria that can ends up with frequent damaging infections in the lungs. In addition mucus build up can prevent necessary enzymes to reach the intestines, and also pancreas problems. Pancreas is an organ that is producing insulin to control the blood sugar level. [3] The best description for CF can be; chronic pulmonary disease with a persistent coughs, elevated sweat electrolytes, and pancreatic insufficiencies that result in mal-absorption and recurrent diarrhea. [4] Debilitating exacerbations of pulmonary infection because of chronic microbial colonization of the major airways is the foremost cause of mortality in patients who they are suffering from cystic fibrosis (CF). The CF patient's lung is the unique environment for microbial pathogens growth. In healthy pulmonary system, inhaled bacteria are doing to a mucus blanket lining the major part of airways and then moved upward by mucociliary clearance, and at the end they will swallowed and destroyed by stomach acids. Bacterial colonization in the CF patient's lung combined the pathophysiological effects of the CF gene defect and pulmonary damage from previous infections with the ability of a relatively narrow spectrum of opportunistic pathogens to overcome normally highly effective lung defenses. [5]
Although multiple microbial species can colonize the CF lung, CF patients are particularly have infected by an alginate secreting bacteria, which is called *Pseudomonas Aeruginosa*, it can be one of the major cause of decline in lung function and death. This opportunistic pathogen (*Pseudomonas Aeruginosa*) produces a number of unique virulence factors that make it particularly adept at infecting specific host tissues such as inflamed lung environment and establishes chronic infections and then it becomes the predominant pathogen in CF. [4] Alginate can significantly increase the elasticity and viscosity of the mucus. [6]
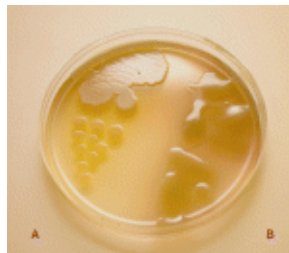

Figure 1.1 Alginate production by P. aeruginosa. Strains were streaked on Luria–Bertani (LB) agar without NaCl and incubated at 37°C for 12 h and at 25°C for 24 h to enhance pigmentation. A. Non-mucoid wild-type PAO1 strain. B. Mucoid CF isolate FRD1 (mucA22). [7]

1.2 Alginate

Hydrogels have a wide record of use in basic sciences, medicine, and pharmacy. [8] Nowadays both synthetic and naturally derived hydrogels have been used as synthetic extracellular matrices for cell immobilization, cell transplantation and tissue engineering. [9] Recently the synthetic ECMs replaced many functions of the native ECMs, such as providing mechanical integrity to the new tissue, organizing cells into a three- dimensional architecture, and providing a hydrated space for the diffusion of nutrients and metabolites to and from the cells. [10]

Alginates are relatively abundant in nature because they arise both as a structural component in marine brown algae (*Phaeophyceae*), comprising up to 40% of the dry matter, and as capsular polysaccharides in soil bacteria. Alginates are naturally occurring polysaccharides synthesized in brown algae and certain types of bacteria and have been extensively used as hydrogel synthetic ECMs. [11] The industrial applications of alginates are linked to its ability to retain water, and its gelling, viscosifying, and stabilizing properties.

1.2.1 Historical Outline

The British chemist E. C. C. Stanford was the first one who described alginate (the preparation of "alginic acid" from brown algae) with a patent dated 12 January 1881. After this patent, the British chemist discovery was further discussed in papers from 1883. Stanford belief was that alginic acid contains nitrogen and it has more contribution on the elucidation of its chemical structure. In 1926, some groups who they were working individually realized that uronic acid was the constituent part of alginic acid. The nature of the uronic acids existing was investigated by three different groups shortly afterwards which they all founded D-mannuronic acid in the hydrolysate of alginate. The nature of the bonds between the uronic acid residues in the alginate molecule was determined to be β1,4, as in cellulose.

However this very simple, acceptable and satisfactory picture of the constitution of alginic acid was, destroyed by the work of Fischer and Dorfel afterwards in 1955. They determined the presence of a uronic acid different from mannuronic acid in the hydrolysates of alginic acid, in a paper chromatographic study of uronic acids and polyuronides. This new-presented uronic acid was identified as L-guluronic acid. The number of L-guluronic acid was considerable, and a method was developed for quantitative determination of mannuronic and guluronic acid.
Alginate then had to be viewed as a binary copolymer composed of α-L-guluronic and β-D-mannuronic residues. As long as alginic acid was observed as a polymer containing only D-mannuronic acid linked together with β -1,4 links, it was sensible to assume that alginates from different raw materials were chemically identical and that any given sample of alginic acid was chemically homogeneous. [12]

1.2.2 Chemical Structure

Alginates are synthesized as a homopolymer polymannuronic acid also known as mannuronan or PlyM [13] Alginates are composed of (1→4)-linked β-D-mannuronic acid (M units) and α-L-guluronic acid (G units) monomers, which

are different in amount and serial distribution along the polymer chain depending on the source of the alginate [14]. The alginate molecule is a copolymer block composed of three regions. Regions of sequential M units (M-blocks), regions of sequential G units (G-blocks),and regions of a tactically organized M and G units. Divalent ion like Ca^{2+} cooperatively can binds between the G- blocks of adjacent alginate chains, and then will create ionic interchain bridges which cause gelation of aqueous alginate solutions. It is important to keep in mind that ionically cross- linked alginates will lose mechanical properties over time in vitro, presumably due to an outward flux of cross- linking ions into the surrounding medium. Figure (1.2) [7].
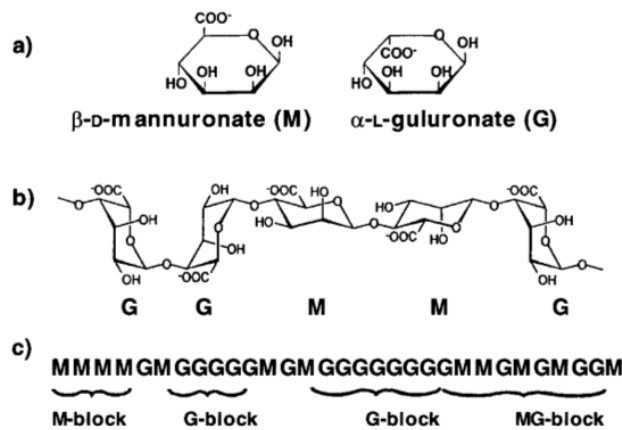

Figure 1.2: Structural characteristics of alginates: (a) alginate monomers, (b) chain conformation, (c) block distribution.

Physical properties of alginates are not only depends on the uranic acid composition but also upon the relative proportion of three types of blocks. The solubility in acid is mainly dependent on proportion of MG blocks in the polymer and gel formation in the presence of calcium ions is particularly depends upon auto-cooperatively formed junctions between the GG blocks. [15]

The ratio between the monomers M and G depends strongly on the relative content of different AlgE epimerizes present in the cells responsible for the biosynthesis of the polymer. Sequences of pure M monomers, a combination of M monomers and G monomers and pure G monomers stretches may occur and are referred as M-blocks, MG-block and G-blocks respectively.

Moreover, and of the great importance in creation of hydrogels, is the alginate chains affinity, i.e. the natural attraction, for divalent ions e.g. Ca^{2+}, Mg^{2+} and Sr^{2+}. Though, divalent ion binding is strongly dependent on the distribution of M and G subunits: While M-blocks have no satisfying binding regions for Ca2+ ions, MG - and G-blocks consist of channels where divalent ions can bind leading to the possibility for cross-links between alginate chains, ultimately facilitating gel creation. The reason is the way of the monomers orientation: Due to the local orientation of the β-D-mannuronic rings, PolyM appears as a rod-like molecule. The α-L-guluronic rings on the other hand, form bonds so that the polymer appears in a zigzag formation, because a chain-like local conformation is favorable due to the different orientation of the COO−-group. Hence, binding

pockets for divalent ions are created so that the ions may bind to the OH- and COO- groups [16].

While both MG-blocks and G-blocks have been shown their ability of forming hydrogels, polyalternating sequences have been considered unable to cooperatively bind Ca^{2+} ions and form connection zones in the same way as G-blocks. These different junctions will have a direct impact on the stability and permeability of gels. GG/GG-junctions, shown in figure (1.3), are the most stable ones and will result in mechanically robust hydrogels. However if the gel consists of high numbers of GG/GG-junctions (for instance if the divalent ion concentration and/or G-block amount is too high), the diffusion rates for smaller molecules, such as insulin, glucose or oxygen, through the gel will be reduced.
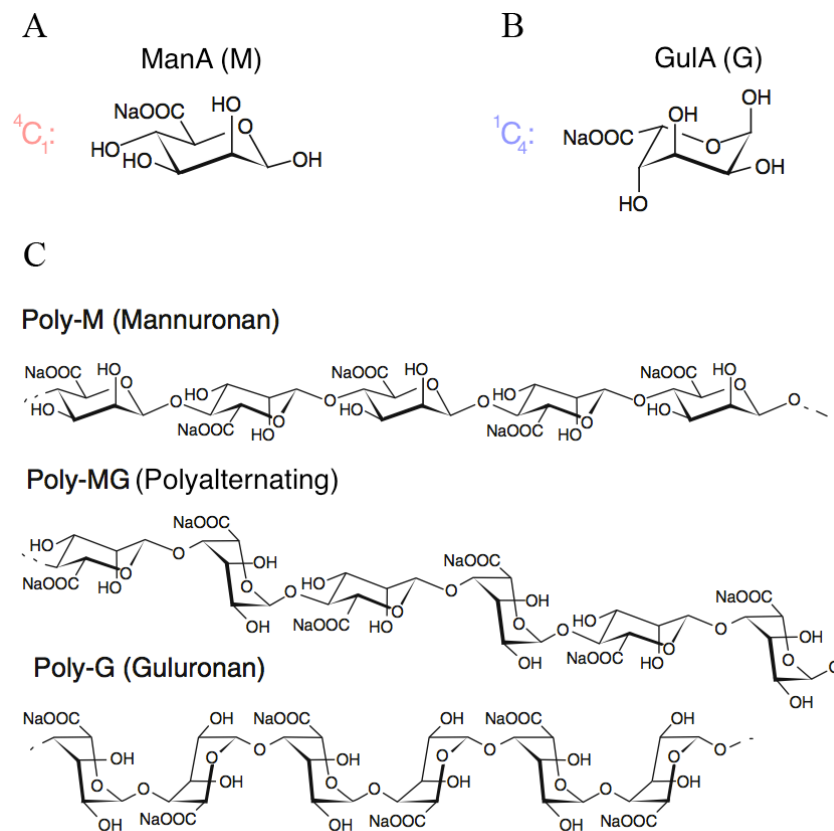
Figure 1.3: **(A)** A β-D-mannuronic ring. **(B)** A α-L-guluronic ring. **(C)** Alginate is initially biosynthezised as a homopolymer PolyM. Strecthes of PolyMG and PolyG may occure after post-polymer epimerization of PolyM carried out by the mannuronan C-5 epimerases.

Alginate chains may be described using the worm-like chain model, which applies for semi-flexible polymers i.e. polymers with a behavior that is characterized as a crossing between a random coil and a stiff rod. The force-dependent extension of apolymer with worm-like characteristics may be written as:

$$\frac{Fl_P}{K_B T} = \frac{1}{4}(1 - \frac{x}{l_0})^{-2} - \frac{1}{4} + \frac{x}{l_0} \tag{2.1}$$

Where F is the force acting on the polymer, l_P is referred to as the persistence length, which is a parameter describing the polymer stiffness, x is the polymer extension, l_0 is the contour length (i.e. the chain length at maximum possible extension), K_B is Boltzmann constant and T is temperature.

The extension is more or less linearly dependent on the force, in the region of low force. In the region of low force, polymers degree of freedom faces a gradual loss (e.g. monomer rotation, back bone configuration and electronic states), the countervailing force is referred to as an entropic force, and the first part of the force vs. extension curve is therefore referred to as the entropic regimen. Having more extension, more than the polymers extent, would ultimately lead to stretching of the polymer backbone. This regimen is hence referred to as the enthalpic regimen, due to a countervailing enthalpic force. [17]

1.2.3 Enzyme Kinetics

Conversion of M- to G- monomers on the alginate chain is one of the many biochemical processes, which they are time-consuming or they are not even possible in absence of catalysts for reaction. By having alginate as a stabilizing biopolymer in certain cell types within evolution led to the biosynthesis of enzymes, which are able to accelerate alginate monomer conversions through non-covalent bond formations by the same reaction condition. From general transition state theory, a chemical reaction can be seen as a crossing of a transition state with an activation energy ΔG. By binding a substrate to active site of an enzyme; the site of the catalytical process is executed, in this case the activation energy is decreased such that the chemical reaction rate is increased by manifold. Through lifetime of the non-covalent bond of enzyme-substrate, the enzyme varies the electronic structure of the substrate by for instance electron transfer, protonation or hydrophobic partitioning. The breakage and rejoin ability of covalent bonds (stronger) over non-covalent interactions (weaker) is due to interplay between all non-covalent forces involved between the enzyme and substrate, for example van der Waals and electrostatic. For an enzyme E that binds to a substrate S to form an enzyme-substrate complex ES that will eventually leads to the creation of a product P, the simplified chemical reaction is as following:

$$E + S \underset{K_a}{\overset{K_d}{\rightleftharpoons}} ES \xrightarrow{K_{cat}} E + P \tag{2.2}$$

Where K_a and K_d denotes respectively the rate of association and dissociation. Catalytic constant is defined as K_{cat}, and represent the maximum number of enzymatic reactions catalyzed per second. Assume that the enzyme [E] concentration is much lower than the substrate concentration [S], and not taking intermediate states or product inhibition (competes with the substrate for the active site) into consideration, the Michaelis Menten equation for the rate of product formation ϑ is:

$$\vartheta = \frac{d[P]}{dt} = \frac{V_{max}[S]}{K_M + [S]} \tag{2.3}$$

$$K_M = \frac{k_d + k_{cat}}{k_a} \qquad\qquad (2.4)$$

Here V_{max} is the maximum reaction velocity at maximum saturation substrate concentration, [P] is the product concentration and K_M is known as the Michaelis constant and is defined as the concentration for which the reaction has reached half of the maximum speed. The more important information which can be find here is that K_M is connected to the substrate's affinity for the enzyme. Realistically, when an enzyme-substrate froms a complex *ES*, the transition from substrate to product may include many steps, for which the enzyme undergoes conformational changes to reduce multiple transition barriers. Hence the constant k_{cat} will become a function of all the rates inbetween every transition from the time the ES complex is formed, until the end product P is created. [18]

1.3 Mucin

Luminal epithelial surfaces of our body are covered by a secreted layer of mucus consisting chiefly of water (95%), high molecular weight polymeric glycoproteins known as mucins (3%), and other small molecules (2%). [19] This layer operates as a lubricant and as a protective barrier shielding epithelial cells from damaging substances. The mucus layer in the stomach faces the severest challenges, not only from ingested materials, but also from the highly acidic gastric juice secreted by the stomach itself. The gastric lumen's pH is typically 1 ≤pH ≤2 during active digestion, whilst the epithelial surface's pH is close to neutral pH, and this gradient is maintained across the mucus layer. The mechanical properties of gastric mucus, are crucial to its protective function and highly relevant to the problem of drug delivery through the mucus layer, are primarily derived from the mucin glycoproteins that form the gel matrix of the mucus.5 Mucins consist of a protein core, with domains rich in cysteine or serine, threonine, and proline, with polysaccharide side chains that account for 80% of the molecular weight. These glycoproteins form large polymeric aggregates up to approximately 20 MDa via disulfide linkages.6 previous studies of the structure and dynamics have led to a model for pH-induced gelation of gastric mucin.

The airway surface liquid (ASL), which covers the epithelial lining of the mammalian airways forms the first track of defense against inhaled pathogens. It develops to be contained of two relatively distinct layers, a watery layer that surroundings the cilia on the apical surface of the ciliated cell, i.e., the periciliary liquid layer (PCL); and a layer that is rich in mucins, the mucus layer, that resides over the PCL. [20] (Figure 1.4)

The mucus layer consists of high molecular weight and heavily glycosylated macromolecules, consists of at least two distinct genes (MUC5AC and MUC5B), which behave as a twisted network of polymers lung defense. This liquid layer is crucial first because it provides a low viscosity solution in which cilia can beat rapidly (about 8–15 Hz) and then because it shields the epithelial cell surface from the overlying mucus layer. [21] Same amount of MUC5AC is available for

both gastric mucus and cystic fibrosis mucus, and also the gene coding for mucus in pig is highly homological to the mucus gene in humans.

Epilethal mucins are glycoproteins with very large molecular weight that they provide the viscoelastic and gel forming properties of mucus, the jellylike protective layer covering epithelial organs. In the mammalian stomach the mucus gel layer protects the fundamental epithelial cells from HCl in the lumen. [22]

The macrostructure of mucus glycoproteins or 'mucins' performs to have a large number of mutual structural features; independent of whether they are gastrointestinal, cervical or tracheobronchial in source. mucins materialize to have a very high molar mass (ranging from 0.5 x lo6 to over 40 x IO6g/mol). Mucins are composed of multiples of a *'basic unit'* of molar mass between 400,000 and 500,00Og/mol that are covalently linked together into linear arrays. The basic unit is prepared from a single chain polypeptide backbone with two distinct regions:

(i) A heavy glycosylated central protein core that a large number of carbohydrate side chains are attached mostly by O-glycosidic linkages through the serine and threonine amino acid residues; followed by (ii) one or two terminal peptide segments frequently referred as a 'naked proteins regions', because these regions are regions of low or even no glycosylation. These basic units are accumulated linearly into *'subunits'* (M-2.5 x 106) and then further by disulphide bridging into the mucin macrostructure. [23]
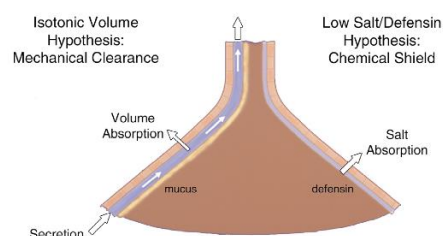
Figure 1.4: Pulmonary defense mechanism is responsible for preventing chronic bacterial infection. The lung is represented as an inverted funnel, reflecting the relative surface area of distal versus proximal airways. The mechanical-clearance-of-mucus hypothesis is shown on the left. The schema portrays discrete mucus and periciliary liquid layers and ascribes to the epithelium a volume-absorbing function. The chemical shield hypothesis is shown on the right, with the epithelium depicted as having a salt but not a volume absorbing function to produce the hypotonic ASL required for defensing activity.

The respiratory mucus as mentioned is a gel or biopolymer composed of a network of high molecular weight glycoproteins, which realizes a multitude of roles, directly or indirectly related to their biochemical and physical properties. One of the main duties ascribed to mucus is to form a continuous filter at the cell-air interface and, therefore, to constitute a barrier, protecting the epithelial cells from invasion and injury by microorganisms and toxic agents present in the environment. Although the most widely studied function of the respiratory mucus is mucociliary clearance, is still a variety of other functions, namely airway hydration, regulation of the periciliary water, bacterial adhesion and clearance, filtration and diffusion barrier, are almost as

important as mucus clearance in the protection of the underlying respiratory cells. All these functions are closely connected to the physical and biochemical characteristics of mucus. [24]

Mucins are categorized in two main groups; membrane-bound and secreted, which share some common features. Membrane bound is further divided into two mucins; namely MUC1 and MUC4, whereas secreted bound are divided into four subclasses; MUC2, MUC5AC, MUC5B and MUC7.Besides this, there are three more types of mucins; MUC3, MUC6 and MUC8, which cannot be classified as either membrane bound, nor secreted. It is known that each human mucin has a counterpart in other animals. [25]
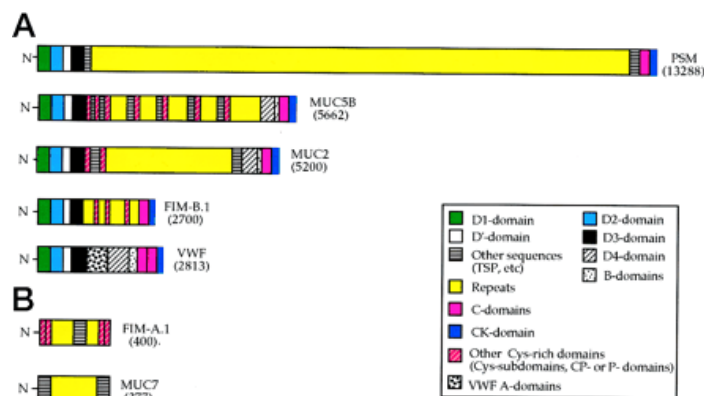
Figure 1.5: A, comparison of the domains in the polypeptide chains of four secreted mucins with the corresponding domains in human von Willebrand factor. B, the domain structures of two small secreted mucins not related to human von Willebrand factor. The complete amino acid sequence of each polypeptide has been established. The number in parenthesis is the number of amino acid residues in the polypeptide. The length of each polypeptide inA is proportional to the number of amino acid residues it contains. The polypeptide chain lengths in A and B are not drawn to the same scale. [26]

1.4 Aim of Study

During this study it is tried to give better understanding details of molecular interaction between alginate and mucin. It is expected that interactions being dependent on structural properties of the biomacromolecules and co-factors existing in solution. Parameters in the energy landscapes of the interactions like the separation distance to barrier and lifetime are expected to reflect such differences. In this thesis, the energy landscapes of interactions between alginates with different monomer sequence and model mucins are determined, including also co-factors that can be expected to enhance their interactions.

2. Single Molecule Measurements

2.1 Single Molecule Force Spectroscopy

Single-molecule experiments can contribute to bridge the gap between physics and biology. Single-molecule experiments offer a new instrument in physical biochemistry that allows scientists to explore biochemical processes at an unprecedented level. They offer a measureable description of biological processes reminiscent of the physicist's approach. Single-molecule experiments are made improvement in nanotechnologies. Combination of these with microscale manufacturing techniques will provide the technology which is required to design and build scientific instruments with high sensitivity and precision to manipulate individual molecules and measure microscopic forces, so allow experimentalists to investigate various physical and biological processes. [27]

One of the great challenges in molecular and structural biology understands the forces that govern on specific molecular interactions. Such specific interactions are outcome of multiple weak, non-covalent bonds that they are produced between defined portions of the interacting molecular partners. In ensemble measurements manipulation of biological complexes at a single-molecular level has lost which is proven to be a very important tool to attain information about e.g. enzyme mechanisms. By applying ensemble measurement user will get a wider picture with the average state of a large number of molecules, where contribution of individual enzymes does not have very significant influence on the outcome. Therefore distributions and averaged parameters are replaced by dynamic. By using this method the dynamic fluctuations that including low lifetime intermediate enzymecomplex stated are undetectable and micro-heterogeneity is masked. In ensemble measurement user would expect average energy state if the enzymes occupy several states and it is because of the unsynchronized energy of enzymes with multiple conformational states. [28] The foremost difference between single-molecule measurements and traditional biochemistry methods is in the kind of average done when measuring the properties of the system. single-molecule measurements allow experimentalists to access biomolecular processes by following individual molecules. By using single-molecule measurement it is possible to measure distributions describing certain molecular properties, characterize the kinetics of biomolecular reactions and observe possible intermediates. Single-molecule measurements provide further information about thermodynamics and kinetics, which is sometimes difficult to obtain in bulk experiments. [27] By using the single molecule measurement synchronization would not be a problem anymore and the reaction sequence of each molecule is observable. [28]
Various techniques have been recently engaged with directly probing weak interactions, including surface force apparatus, pipette suction, magnetic beads, flow chamber apparatus, and optical traps and tweezers. The techniques of using optical traps have been particularly well liked in view of their high force sensitivity. The drawbacks of the optical trap-based apparatuses are in the limited range of samples amenable to analysis (biopolymers must be generally longer than $\sim2\,\mu m$), and general unsuitability for applying forces greater than

~150 picoNewtons (pN). By arrival of the probe microscopes, and specifically the atomic force microscope (AFM) has opened new horizons in force measurements. [29]

The importance of forces in biology has been recognizable for quite a while but only in the past decade we have acquired equipment and methodology to directly measure interactive forces at the level of single biological macromolecules and/or their complexes. This study focuses on force measurements performed with the atomic force robot JPK 300.

2.2 Dynamic Force Spectroscopy

Dynamic force spectroscopy has been introduced as a spectroscopic implement to investigate the complex relationships between "force-lifetime and chemistry" in single molecules bound in an adhesion complex and to uncover details of molecular scale energy landscapes and adhesion strength, in other word it is introduced to help getting deeper understanding of interactions between biological complexes through single molecule measurements. [30] A model that can predicts the distribution of rupture forces, the corresponding mean rupture force, and variance, which they all are amenable to experimental tests is called dynamic force spectroscopy of single molecules. [31]

For measuring the rupture force in dynamic force spectroscopy one need to quantify the maximum extension of a spring, the linker, which is followed by rapid recoil of the spring to its rest position. By looking at this property it will resembles the stick-to-slip transition in studies on friction. For studying the unbinding process of single molecule one studies one molecule at a time that that is meant one measures a collection of independent rupture events. This will lead to a rupture forces distribution. Furthermore the exploration of the energy landscape of the bound complex is by the measurements of rupture forces over a wide range of pulling velocities, ranging from very slow to extremely fast. In dynamic force spectroscopy experiments, by pulling a spring from its equilibrium state at a given velocity the adhesion bond can be driven. Adhesion bonds rupture occurs by use of thermally assisted escape from the bound state across an activation barrier. By increasing the applied force the rupture force will be determined by a relationship between the rate of escape in the absence of the external force and the pulling velocity (loading rate). Accordingly, it is stated that the measured forces are not an intrinsic property of the bound complex, but they are dependent on the mechanical setup and loading rate, which are applied to the system.

By considering a one dimensional description of the unbinding process along the axis x which is the single reaction coordinate, the dynamic response of the bound complex is determined by the Langevin equation as following:

$$M\ddot{x}(t) = -\gamma_x \dot{x}(t) - \frac{\partial U(x)}{\partial x} - K(x - Vt) + \xi_x(t) \qquad (2.1)$$

In the above mentioned equation M is mass of molecule and K is representing the spring constant for velocity of V. Adhesion potential is defined as $U(x)$, γ_x is a

dissipation constant and the effect of thermal fluctuations is given by a random force $\xi_x(t)$, which is δ- correlated $< \xi_x(t)\xi_x(0) >= 2K_BT\gamma_x\delta(t)$. In equation (2.1) the thermal fluctuations are the origin of the distribution of rupture forces. In a more general case other sources of randomness are possible.

The bound state is defined by the minimum of the total potential as stated in the following equation:

$$\phi(X,t) = U(x) + \frac{K}{2}(x - Vt)^2 \tag{2.2}$$

Unbinding event occurs in the absence of thermal fluctuations when the potential barriers disappear, for example at the instability point where $\frac{d^2\phi(x,t)}{dx^2} = 0, \frac{d\phi(x,t)}{dx} = 0$. At this point the spring force, $F = K(x–Vt)$, will reach to its maximum value and $F = Fc$. If the fluctuations present in the system the escape from the potential well occurs earlier, and the probability of molecule persistence in its bound state is defined by Kramers' transition rate and can be approximately calculated through the following kinetic equation:

$$\frac{dW(t)}{dt} = -\frac{\Omega_1(t)\Omega_2(t)M}{2\pi\gamma_x}\exp[\frac{-\Delta E(t)}{K_BT}]W(t) \tag{2.3}$$

In the above mentioned equation W(t) is the probability of molecule persistence in its bound state and $\Delta E(t)$ is the instantaneous barrier height, $\Omega_1(t)$ and $\Omega_2(t)$ are the effective oscillation frequencies at the minimum corresponding to the bound state and $\phi(x,t)$ maximum of the combined potential. This equation will not take place in account rebinding processes. The experimentally measured rupture forces distribution can be expresses in terms of W as following:

$$P(F_{max}) = -\frac{d}{dF_{max}}W(F_{max}) \tag{2.4}$$

$$< F_{max} >= -\int_0^\infty F_{max}(\frac{d}{F'_{max}}W(F'_{max}))dF'_{max} \tag{2.5}$$

$P(F_{max})$ is the experimentally measured distribution of rupture forces. As it is mentioned before F_{max} is the rupture force, and it is defined as the maximal spring force $K(x–Vt)$, will be measured during rebinding process.
The unbinding rate is exponentially dependent on the $\Delta E(t)$ the focus is on value of F close to the critical force, F_c where the barrier will disappear completely. The oscillation frequencies and the instantaneous barrier height will be calculated in terms of the reduced bias, $\varepsilon = \frac{1-F_{max}}{F_c}$ as following:

$$\Delta E(t) = U_c\varepsilon^{3/2} \qquad , \Omega_{1,2}(t) = \Omega_c\varepsilon^{1/4} \tag{2.6}$$

Here U_c and Ω_c are the parameters for the bare, unbiased, potential $U(x)$. [32]

3. Theory of Single Molecule Pair Unbinding

3.1 Historical Outline

In 1978 Bell talked about "how chemical bonds are affected under the influence of and external force" [33] his theory was the begging of Evan Evans and Ken Ritchie's Theory of single molecule pair unbinding at the end of 20th century. Moreover, the theory of forward escape rate described by Kramers in 1940 [34], which again had its outspring in the more general Fokker-Planck formalism, is included in their work.

3.2 Free Energy Landscape

For understanding the underlying nature of single molecule interactions it is crucial to know the information concerning the way of creation and breakage of chemical bonds. Molecules can form advanced biological complexes with many possible conformational states over non-covalent bonds and each state of them is connected to a free energy. Therefore free energy landscape term is used to describe transitions between these states.

The total degree of freedom has influence on the free energy landscape of biological complexes, for example monomer rotation, backbone configuration and electronic states. The N-vector $\vec{x_n}$ defines a systems total depth of field:

$$\vec{x}_n = \{x_1 + x_2 + \cdots + x_n + t\} \tag{3.1}$$

x_1, x_2, x_n are independent variables in equation (3.1). In a system contains molecules ensemble, each of them characterized by its d.o.f, both the energy **E** and the momentum **p** are conserved.

The system is freely diffuse along the free energy surface $G(\vec{x}_n)$, from the time when it is energetically beneficial, the system spend more time around the minima's of this surface.

Protein folding has been subject of many studies during past decades. By simple words, folding can be described as a process that many existing degree of freedoms in unfolded polypeptide chains will become coordinate into well-defined structures by means of energetics specifics to their sequences of amino acid. The required information about protein folding is energy of every relevant protein conformation and the motion which is involved in changing conformation. [35]

Great amount of depth of field (d.o.f) for unfolded polypeptide chains, $\sim 10^{143}$ conformational states are possible this theory introduced by Cyrus Levinthal in 1969, and it is known as Levinthal paradox. [36] Much more has been written about Levinthal paradox and its numerous resolutions. The paradox is done when there is not sufficient time to search randomly the entire conformational space available to a polypeptide chain as an unfolded protein. Levinthal's point was that proteins have to fold through some direct processes. [37]

It is therefore common practice to project the system onto one curvilinear coordinate called the *'reaction – coordinate'*, x. Focusing on one-dimensional motion along a one-dimensional surface is considerably less comprehensive. However, it has to be accepted in mind that Z hidden d.o.f is lost by making this assumption. For this reason, a given one dimensional "particle" (as shown in Fig.(4.1B)) which is confined by the 1-D free energy surface G**(x)**, will be able to exchange energy and momentum with its surroundings through friction and fluctuation. In this case, E and p are not conserved. The dynamic development of the localization x**(t)** of the particle is given by the over damped Langevin equation of motion:

$$\frac{d\vec{x}}{dt} = \frac{D}{k_B T}\left(\vec{F} - \nabla G(\vec{x}) + \delta\vec{f}\right) \tag{3.2}$$
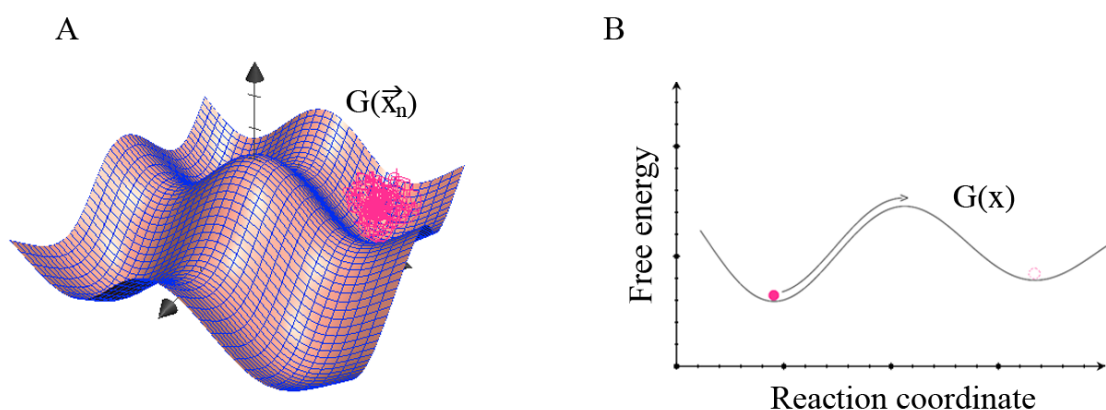

Figure 3.1 (A) An arbitrary free energy surface $G(\vec{x}_n)$ with an arbitrary system diffusing within one of the minimas. (B) Particle in a 1D free energy surface G(x)

In equation (4.2) D is stated as diffusion constant , F is the external deterministic force, ∇G($\vec{x}$) is representing the local gradient felt by the 1-D particle and $\delta\vec{f}$ describes the random force representing the uncorrelated thermal impulses, obeying the fluctuation dissipation theorem.

3.3 The Two Stated Model

Folding's of some proteins turn to be a two-state kinetic process. We must be careful about the meaning of ''state''. It signifies a region of configuration space, usually the neighborhood of a potential minimum. The intrinsic state is associated with the deepest minimum and the ''unfolded state'' is the rest of configuration space. A two-state kinetic model is acceptable if protein molecules rapidly equilibrate between different unfolded conformations prior to complete folding. This rapid equilibration is the natural consequence of reasonable assumptions of reaction rate constants and folding thermodynamics. [38]

The easiest example of system that can be pronounced by the two-state model, is the hairpin folded proteins or hairpin folded DNA (Fig.(4.2)). Not taking the low-

lifetime intermediate states into account, only two states are possible for the hairpin folding system: folded or unfolded. [39]
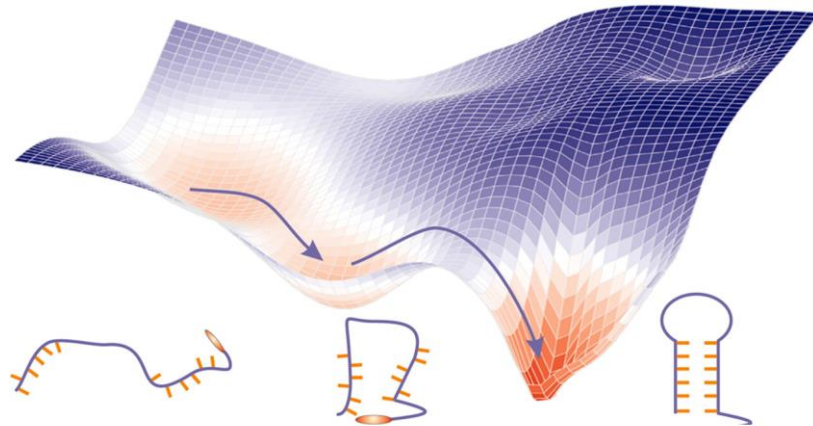
Unfolded ensemble   Intermediate ensemble   Folded structure

Figure 3.2 The Picture shows the landscape of DNA hairpin folding and melting. The free-energy surface with multiple global minima depicts folded, collapsed (compact) intermediate and single-stranded structures. This image is indicating the different structures as well. [39]

The two-state model can simplify the multi-barrier systems into a series of two state transitions as shown in Fig.(4.3). This method enables the study of complex transitions by breaking them down to more easily solved problems. The two-state model can be divided into an initial state A, a transition state t and a final state B, each with its free energy (G_A, G_t and G_B, respectively) as shown in Fig.(4.3). An activation energy $\Delta G_{tA} \equiv (G_t - G_A)$ is needed to be able to overcome the energy barrier like cross the transition state.
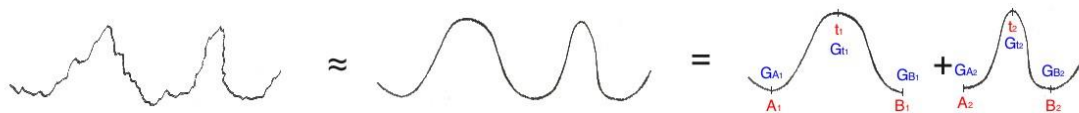
Figure 3.3: A complex multi-barrier system simplified and split into two separate two-state systems.

A comparison can be done between a system with 1D particle bound by a free energy surface and a chemical reaction system in a liquid environment.

$$A \rightleftharpoons B \; ; \; K_{eq} = \frac{[B]_{eq}}{[A]_{eq}} \tag{3.3}$$

In the abovementiond reaction A is the start compound and B is the final compound, where $K_{A \rightarrow B}$ is the rate of forward reaction and rate of backward reaction is represented by $K_{B \rightarrow A}$, K_{eq} is stated as the equilibrium constant and [A] and [B] representing the compound concentrations of A and B in equilibrium.

The two stated model would be more realistic if one considers the depth and curvature of the wells and peaks of the energy surface.

15

By looking at figure 4.3 as an example one can consider if the well A width is increased the forward rate is decreased, because particles for reaching state B need to travel greater distance. If one considers that particle move slower than the decrease in forward rate is again expected. By considering mentioned parameters new expression will be as follow:

$$K_{A \to B} \sim \frac{K_B T}{\zeta l_t l_A} e^{-\frac{\Delta G_{tA}}{K_B T}} \tag{3.4}$$

in the abovementioned expression l_A and l_t are the well and peak width respectively within $\frac{1}{2} K_B T$ of the maximum and the minimum energy values. ζ defines the fractional coefficient and ΔG_{tA} is the activation energy.

3.4 Applied Force on Free Energy Surfaces

For better understanding the bond dissociation, one must first understand how free energy surface will respond to an applied external force f. It is noticeable that the free energy expression will take the bellow form:

$$G(f, x) = G_0(x) + \{Effect\ of\ external\ force\} \tag{3.5}$$

In the above mentioned equation $G_0(x)$ is the free energy before external force applied. If one assumes that the force f is applied directly along the reaction coordinate of x then the equation will take the form of:

$$G(f, x) = G_0(x) - f x_\beta \tag{3.6}$$

And

$$x_\beta = < (x_t - x_A) cos\theta > \equiv \Delta x_{tA} cos\theta \tag{3.7}$$

and is referred to as the thermally averaged projection of a energy barrier along the direction of the applied force. The external force of f tilts the free energy landscape as shown in figure (3.4). The wells in free energy surfaces are assumed to be sharp and harmonic for simplicity reasons. This way, x_A, x_t, x_β remains unchanged, thus l_A and l_t also remains unchanged. The only changing factors are the free energies G_A, G_t, G_β, meaning that only the exponential term of the forward rate form (3.4) is affected. The activation energy becomes:

$$\Delta G_{tA}(f) = \Delta G_{tA}(f = 0) - f x_\beta \equiv \Delta G_{tA}^0 - f x_\beta \tag{3.8}$$

Inserting (3.8) will take the form of:

$$k(f) = k(f = 0) \exp(\frac{f}{f_\beta}) \equiv k^0 \exp(\frac{f}{f_\beta}) \tag{3.9}$$

for the bond dissociation rate $k(f)$ with applied force, where k^0 is the same rate as in (3.4). The zero is only a reminder that this rate is independent of the applied force f. In fact, the rate at zero force can be associated with the lifetime time of the bound complex $(\tau^0 = \frac{1}{k^0})$ without external disruption. The parameter f_β, referred to as the characteristic scale for force by the ratio of thermal energy to the distance x_β is defined as

$$f_\beta = \frac{K_B T}{x_\beta} \tag{3.10}$$

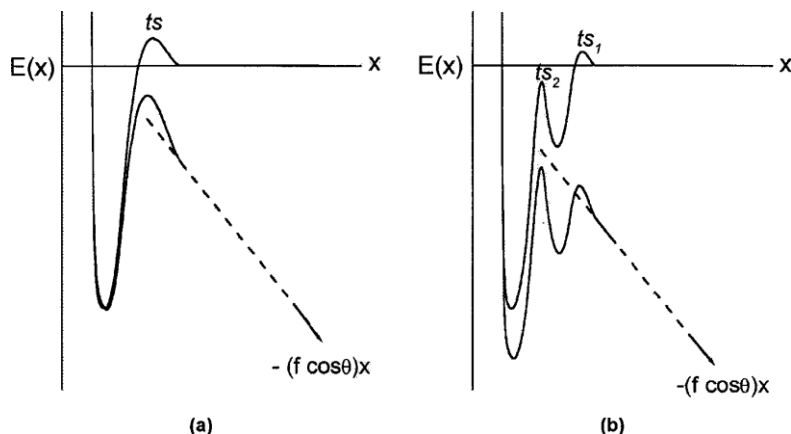**Figure 3.4** : Conceptual energy landscapes for bonds confined by sharp activation barriers transition states (ts). Oriented at an angle θ to the molecular coordinate x, external force f adds a mechanical potential $-(f.cos\theta)x$ that tilts the landscape and lowers barriers. (**a**) A single barrier under force. (**b**) A cascade of barriers under force where an inner barrier emerges to dominate kinetics when the outer barrier falls below by $\sim K_B T$. [40]

Non-covalent interactions have a finite lifetime; so spontaneous unbinding events are possible and can occur without external influences. One consequence of this is that if for instance the force f works very slowly on the system ($\frac{df}{dt}$ is small), fluctuations may cause the bond to break without the applied force contributing significantly to the event. On the other hand, if the force f acts fast ($\frac{df}{dt}$ is big), there is no time for the fluctuations to act, and the contribution from the applied force in the unbinding process will be larger. In other words, the loading rate of the force, defined as:

$$r_f = \frac{df}{dt} \tag{3.11}$$

has a countless influence on how the system is affected by the external force.

By studying the kinetics of bond dissociation in a two-state model approximation, the first order differential equation can be set up:

$$\frac{dP_A(t)}{dt} = -k_{A \to B} P_A(t) + k_{B \to A} P_B(t) \tag{3.12}$$

If the thermal force is smaller than the applied force, forward rate will increase and the backward rate is dropped. So the process is *quasi-adiabatic* and the second part of

17

equation (3.12) will disappear, and P_A is as given below:

$$P_A(t) = \exp[\frac{k^0 f_\beta}{r_f}(1 - \exp\left(\frac{r_f t}{f_\beta}\right)] \tag{3.13}$$

Transition probability from A to B in the time interval of t and t+dt is $P_{A \to B}(t + dt)$ can be written as:

$$P_{A \to B}(t + dt) = probability\ of\ finding\ the\ system\ in\ state\ A\ to\ begin\ with$$
$$.probability\ of\ a\ bond\ dissociation \tag{3.14}$$

$$\frac{P_{A \to B}(t+dt)}{dt} \equiv P(f) = k^0 \exp\left(\frac{f}{f_\beta}\right)\exp[\frac{k^0 f_\beta}{r_f}\left(1 - \exp\left(\frac{f}{f_\beta}\right)\right)] \tag{3.15}$$

$P(f)$ is the probability density and can be found as the abovementioned equation.

The most probable unbinding force is f^*, can be estimated by having the maximum value for the distribution of lifetimes:

$$\frac{dP(f)}{df} \equiv f^* = f_\beta \ln\{\frac{r_f}{k^0 f_B}\} \tag{3.16}$$
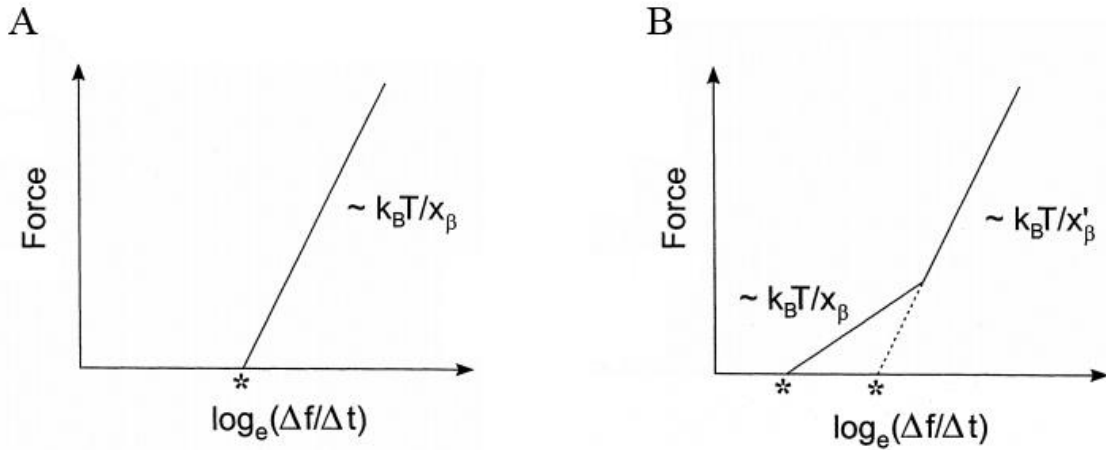
Figure 3.5: Dynamic strength spectras for the corresponding energy diagrams in Fig.(3.4). Reproduced from [41].

Slopes in Figure(3.5) indicating the dominating energy barriers location, and are given according to (3.10). Presence of second energy barrier will make a change in slope, as illustrated in Figure (3.5b). The distance x_β decreases with increasing slope steepness so the position x_β of the inner barrier would be related to the steepest slope. This can be seen by comparing the two slopes in Figure(3.5b) with the two corresponding energy landscapes in Figure(3.4b). Furthermore, k^0 is obtained when extrapolating the most probable unbinding force to zero force ($f^* = 0, r_f = r_f^0$), following the relationship:

$$k^0 = \frac{r_f^0}{K_B T} \tag{3.17}$$

3.5 Application of Theory

Experimentally, interactions between biological complexes can be seen as force curves; curves with force jumps containing information about the magnitude of the force needed to pull apart the complex, as well as the corresponding loading rate. From analysis of numerous force-curves a force vs. $\log_e$ (loading rate) plot can be obtained. The plot is divided into sub distributions with constant mean loading rates $< r_f >$. To each sub distribution a histogram is created for which the Bell-Evans relation is fitted as illustrated in Figure(3.6).
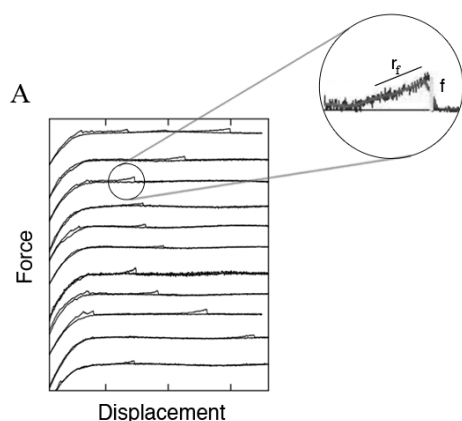
Figure 3.6: A gallery of experimentally obtained force-curves. Each curve contains one to several force jumps each with a magnitude of the rupture force f, as well as the corresponding loading rate r_f

From these fits, parametric values of f^*, x_β and k^0 can beobtained. The dynamic strength spectrum is obtained by plotting the f^* values vs. the corresponding $< r_f >$ and fitting to these values, yet again revealing the parametric values of x_β and k^0. The x_β and k^0 values obtained from each histogram should ideally coincide with the ones obtained from the dynamic strength spectrum. Generally, the parametric values obtained from the dynamic strength spectrum are more reliable than the values obtained from the individual fits due to an averaging.

The reliability of the fits of Bell-Evans expression is connected to the amounts of data points i.e. force jumps, which sets the criteria for the sizes of the sub distributions. Ideally, enough data points are desired to make the sub distributions as narrow as possible (discrete $\rightarrow$ continuous $< r_f >$). Moreover, sub distributions with lack of data points will often result in a fit of Bell-Evans relation, which is dependent on the number of bins of the histogram as shown in Figure (3.7). Thus, the parametric values f^*, x_β and k^0 become dependent on the number of bins. In the case of too few data points, a sacrifice has to be made where the width of each sub distributions is made large enough to avoid bin dependent fits.
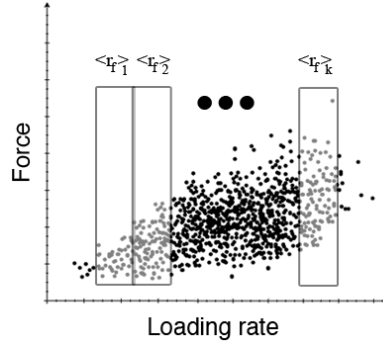
Figure (3.7): The force loading rate plot is divided into k sub distributions with mean loading rates $< r_f >$.

3.6 Analytical Determination of Force Dependent Lifetime

The expression, which was shown in previous sub-chapter (3.9) is indicating a special case for the forward rate where the energy barriers or wells are considered sharp and harmonic. The below expression is for the situation when more complex landscapes are accommodated [42]

$$\frac{1}{k(f)} = \tau(f) = \tau^0 (1 - \frac{v f x_\beta}{\Delta G})^{1-\frac{1}{v}} \exp(-\frac{\Delta G}{K_B T} \left(1 - \left(-\frac{v f x_\beta}{\Delta G}\right)^{\frac{1}{v}}\right)) \qquad (3.18)$$

Here $\tau(f)$ is the force dependent lifetime, τ^0 is when the life time is at zero force and ΔG is the free energy of activation when there is no external force. v is related to the nature of energy surface, when $v =1$ the energy landscape has sharp and harmonic wells or barriers, $v =1/2$ is related to energy landscape with cusp-like barriers and harmonic wells or cusp-like wells with harmonic barriers and when we face to $v =2/3$ the wells and peaks have linear and cubic terms.

4. Materials and Methods

4.1 Mucin Sample

Same major of MUC5AC is available in both gastric mucus and cystic fibrosis mucus, and also the pig gene is highly homologically same as human.
The pig gastric mucin, which is used in this experiment, is obtained from the cardia and fundus of pigs that they are slaughtered recently. For obtaining the crude mucin sample first it is necessary to rinsing the pig stomach to have a clean stomach from food debris and it is done by cold tap water. After that with a microscope slide the stomach is scraped.

Homogenization process is done for the sample, it is immersed for 1 min in 67 mM pH 6.5 phosphate buffer that is including proteolytic inhibitors (1 mM iodoacetamide, 100 mM aminocaproic acid, 10 mM EDTA, 10 mM N-ethylmaleamide, 5 mM benzamidine HCl and 1 mM phenylmethyl-sulphonyl-fluoride) and after this step the sample is centrifuged (9000 rpm, 4 °C, 1 hour) to remove insoluble material. Next the supernatants were collected and purified by CsCl equilibrium density gradient centrifugation (1.42 g/ml starting density). The mucin-rich fractions have a density between 1.45 and 1.49 g/ml, they were pooled, dialyzed (dialysis against de-ionized water (resistivity 18.2 MΩ cm, prepared using a MilliQ-unit, Millipore, referred to as Mq water in the following)), freeze-dried and stored at -20 °C.

4.2 Pseudomonas Alginate Sample

The pseudomunal alginate which is used in this experiment is the high molecular weight pseudomonal alginate sample, PF83, polyM, with a fraction of mannuronic acid equal to 1.0, and a fraction of acetyl groups, present as substitutions on the mannuronic acid, equal to 0.45.

4.3 High-G and Mid-G Alginate Samples

Commercial alginates are produced mainly from Laminaria hyperborea, Macrocystis pyrifera, Laminaria digitata, Ascophyllum nodosum, Laminaria japonica, Eclonia maxima, Lessonia nigrescens, Durvillea antarctica, and Sargassum spp. Table (4.1) gives some sequential parameters (determined by high-field NMR-spectroscopy) for samples of these alginates. The composition and sequential structure may, however, vary according to seasonal and growth conditions. High contents of G generally are found in alginates prepared from stipes of old Laminaria hyperborea plants, whereas alginates from A. nodosum, L. japonica, and Macrocystis pyrifera are characterized by low content of G-blocks and low gel strength.[43]

Table 4.1: Composition and sequence parameters of algal alginates

Source	F_G	F_M	F_{GG}	F_{MM}	$F_{GM,MG}$
Laminaria japonica	0.35	0.65	0.18	0.48	0.17
Laminaria digitata	0.41	0.59	0.25	0.43	0.16
Laminaria hyperborea, blade	0.55	0.45	0.38	0.28	0.17
Laminaria hyperborea, stipe	0.68	0.32	0.56	0.20	0.12
Laminaria hyperborea, outer cortex	0.75	0.25	0.66	0.16	0.09
Lessonia nigrescens[a]	0.38	0.62	0.19	0.43	0.19
Ecklonia maxima	0.45	0.55	0.22	0.32	0.32
Macrocystis pyrifera	0.39	0.61	0.16	0.38	0.23
Durvillea antarctica	0.29	0.71	0.15	0.57	0.14
Ascophyllum nodosum, fruiting body	0.10	0.90	0.04	0.84	0.06
Ascophyllum nodosum, old tissue	0.36	0.64	0.16	0.44	0.20

These data (Table 4.1) are provided by Bjørn Larsen.

In this study the alginates which are used, are High G alginate from Laminaria Hyperborea stipe with notation of LF 10/60 and Mid-G alginate from Macrocystis Pyrifera with sample notation M Pyr. Their specifications are listed below in the table (4.2)

Table 4.2: Alginates specifications

Sample	F_G	F_M	F_{GG}	F_{MG}	F_{MM}	F_{GGM}	F_{MGM}	F_{GGG}	$N_{G>1}$	$[\eta]$ (mg/ml)	M_W (g/mol)
LF 10/60 S12727	0.65	0.35	0.53	0.12	0.23	0.049	0.10	0.48	11	585	113500
Ny M.pyr (MP Biomedical)	0.38	0.62	0.19	0.20	0.42	0.04	0.18	0.15	5	1005	220000

These data (Table 4.2) are given by Biotechnology department of NTNU.

4.4 Immobilization of Pig Gastric Mucin and Alginate

The PGM molecules were covalently linked to the freshly cleaved mica surfaces and alginates to the AFM.
Briefly, the mica surface need to be cleaved and the clean side should be up, then freshly cleaved mica was immersed in 1:1 v/v solutions of MeOH/HCl, for 30 minutes, to make sure the cleanliness of mica surface, rinsed in Mq-water and immersed in a freshly prepared 1% (v/v) solution of trimethoxysilylpropyl-diethylenetriamine in 1 mM acetic acid for 20 min at room temperature, then again rinsed using Mq-water. The result is amine-terminated surface. EDAC was used to precipitate peptide bond creation in the solution of different concentration of Mucin and boric acid. The PGM molecules were conjugated to the mica surfaces by overnight incubation in a solution of PGM in 50 mM boric acid pH 5.8 and 0.5–2.0 mg/ml EDAC.

In analogous manner, the AFM tip (OTR4-10, Veeco, triangular, nominal spring constant 0.02 and 0.08 nN/nm) was used for covalent coupling of the alginate. AFM tip was first cleaned with the same procedure as mica surface cleaning (immersed in 1 : 1 v/v solutions of MeOH/HCl, 30 minutes), amino-silanized by freshly prepared 1% (v/v) solution of trimethoxysilylpropyl- diethylenetriamine in 1 mM acetic acid, it was incubated for 20 min and then rinsed in Mq-ionized water. The alginate molecules were covalently attached to the aminosilanized AFM tips employing a water-soluble carbodiimide (different concentration of alginate, 0.5-2 mg/ml EDAC in 50 mM boric acid, pH 5.8) and kept in the solution for an overnight incubation.

Table 4.3: Different concentration of Mucin and High-G Alginate that were used in this study.

Mucin (mg/ml)	0.01	0.03	0.05
High- G Alginate (mg/ml)	0.02	0.06	0.1

Table 4.4: Different concentration of Mucin and Mid-G Alginate that were used in this study.

Mucin (mg/ml)	0.01	0.03	0.05
Mid- G Alginate (mg/ml)	0.02	0.06	0.1

Table 4.5: Concentration of Mucin and pseudomonas Alginate that were used in this study.

Mucin (mg/ml)	0.05
Pseudomonas Alginate (mg/ml)	0.1

4.5 Measurements

Measurements were carried out using the AFM ForceRobot 300 system (JPK instruments AG, Berlin, Germany), equipped with a JPK precision mapping stage and a liquid cell. In the first part of measurements the data were collected in the liquid cell (aqueous 25 mM HEPES buffer, 150 mM NaCl, pH 6.9) and for the second part data were collected in four different liquid cells first one same as liquid cell in the first part of measurement, second liquid cell was (aqueous 10mM EGTA in 25 mM HEPES buffer, 150 mM NaCl, pH 6.9), third one was (aqueous 1mM Ca^{2+} in 25 mM HEPES buffer, 150 mM NaCl, pH 6.9), fourth one was (aqueous 1mM Ca^{2+} and 10mM EGTA in 25 mM HEPES buffer, 150 mM NaCl, pH 6.9) at room temperature. Before each series of measurements the spring constant of the AFM tip was calibrated using the method of thermal fluctuation of the cantilever using the instrument software. For each PGM–alginate sample investigated, forced unbinding data were collected from 360 unbinding experiments from a series of 10 trials (force curves obtained using a

z-piezo translation of 3–4 mm, 0 s contact time, retraction speed $2\,mm/s$ corresponding to the force loading rate of 50–300 nN/s applied to the samples) in 36 predetermined locations (6*6) evenly distributed across an area of 10*10 mm^2 on the sample surface.
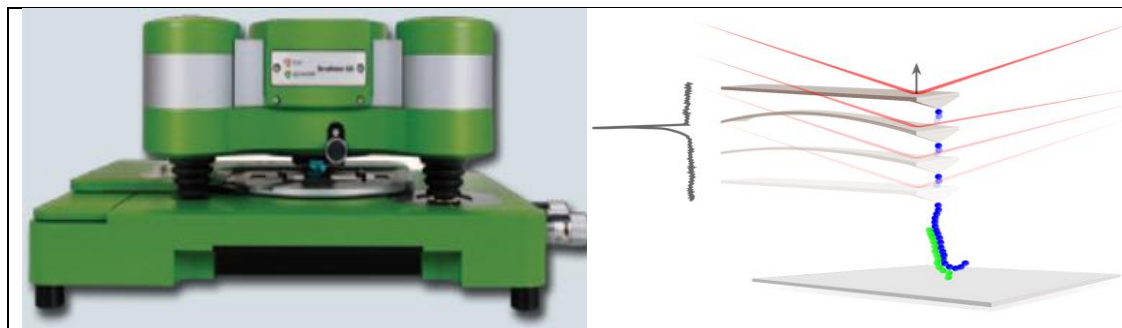

Figure 4.1: The left hand picture shows the AFM ForceRobot 300 system (JPK instruments AG, Berlin, Germany) which is placed in Biophysics Laboratory in Physics Department of NTNU. The right hand illustrates the unbinding event.

Furthermore, the measured interactions should reflect interaction forces between single molecules. It is, however, often hard to determine if a force-curve represent single or multiple interaction events. As a rule of thumb, to avoid multiple interactions, data from experiments where force jumps were frequently large, were not collected. It is the reason of having samples with very low concentration to avoid multiple interactions more.

4.6 Force Robot JPK 300

Scanning probe microscope (SPM) defines a broad group of instruments used to image and measure properties of material chemical and biological surfaces. SPM images are obtained by scanning a sharp probe across surface while monitoring and compiling the tip-sample interactions to provide an image. The two primary forms of SPM are scanning tunneling microscopy (STM) and atomic force microscopy (AFM).[44]

Atomic force microscopes (AFMs) move a sharp tip attached to a soft cantilever in a TV-raster-like pattern over a surface and record deflections of the tip that correspond to the surface topography. When operated in physiological solutions, an AFM allows biomolecules to be observed in their native environment. Progress in instrumentation, sample-preparation methods and recording conditions has provided images of biomolecules and their assemblies that reveal submolecular details. In addition, the AFM allows conformational changes to be observed directly.[45]

Beyond the topographic imaging, AFM has been used to measure and map many types of surface forces and local mechanical properties. A wealth of new information about single molecules has provided us with new insights into intermolecular forces, and the underlying molecular mechanism. [46]

Recently, a new technique single molecule force spectroscopy by AFM has been implemented and opens the possibility for directly measuring the deformation of single polymer chains. It expands the existing spectrum of single-molecule techniques towards lower forces and smaller molecules. [47]

Polysaccharides are essential components of all living organisms and are the most abundant class of biological molecules. The mechanical properties of polysaccharides and their structural origin are of great interest, but these studies have lagged well behind those of proteins and nucleic acids. [48]

Force spectroscopy is a single molecule technique that allows the real-time study of molecular interactions on the nanoscale. Originating from the broad field of Atomic Force Microscopy, force spectroscopy provides the necessary sensitivity to characterize biomolecular interactions such as the unfolding forces of single proteins or forces of a single chemical bond.

For the very first time, the automation of force spectroscopy makes it fast enough to deliver high quality data in short time-frames. A large variety of accessories makes the system most flexible.

4.7 Analysis

The programs, which were used to analyze the obtained single-molecule interaction data, were developed in IDL and MATLAB.

4.7.1 Data Collection

The IDL program used for the analysis of the raw force-jump data *ForceSpecAnalys*; was developed by Professor Bjørn T. Stokke, NTNU, and Trondheim. All force-curves obtained experimentally from the force robot need to be converted to textfile by a special programmed written for force robot curves *JPK Data Processing*. Some of the curves have both multiple and single molecular interactions one should keep in mind to do not choose the force jumps which are indication multiple molecular interactions. Curves, which are obtained, may have one or more force jumps or may be flat. One needs to identify the interesting curves such as curves with force jumps reflecting forced disruption of single molecule bonds. For choosing right force jumps a manual filtration of the curves was done, as the first step of the analysis. The chosen curves with chosen force jumps gives the ideal data points. The program enables collection of rupture forces and the corresponding loading rates. The program also provides a baseline, which is used to determine the force magnitudes. Data points will be analyzed again in other versions of IDL program to give the x_β, τ or k^0 and ΔG for three different υ parameters. Criteria's for the calculated regression and the baseline, as well as other accommodated factors. Each time a force jump was collected; several elements had to be accounted for to make sure the correct values for the loading rates and the force magnitudes were chosen:

Indicate the location of the force jumps (by applying the derivative of the regression line)

choose the relevant force jumps and make sure the baseline does not deviate due to interactions on the end of the displacement plot (the baseline is created based on the last region of the displacement plot)

If the previous point is fulfilled: Choose a displacement range for calculation of the loading rate. The loading rate values were only chosen if they remained constant for different chosen ranges i.e. if they were independent of small variations close to the force rupture. And, if the range was small enough to reflect the actual curvature of the rupture curve (long displacement ranges would yield too much averaging).

For higher forces, force jumps are chosen based on the curvature: Only force jumps that reflect an enthalpic regimen are chosen. This is necessary to avoid multiple interactions since multiple interaction force jumps, in contrary to a stretched single polymer, are consequences of multiple bound polymers for which some are only stretched a little (entropic regimen) and others are stretched beyond their extent. Therefore, although the force magnitude might be relatively high, the force jump curvature does not reflect an enthalpic regimen and the jumps is as a consequence not collected.

Write chosen data points to a separate file.

4.7.1 Bell Evans Method
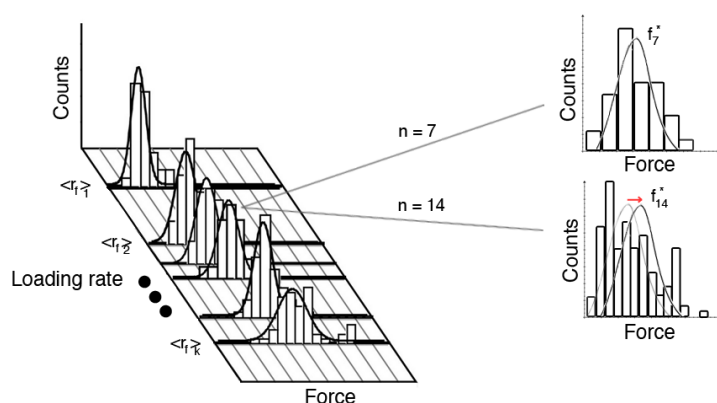
Figure 4.2: Histograms are then made for each sub distribution, for which a fit of $P(f)$ is created and the f^* values (amongst other parameters) are found. If a sub distribution has a lacks of data points, the fit of $P(f)$ becomes sensitive to the number of bins.

Additional analysis were carried out using the program SubDist, which was createdand developed by Armend Gazmeno Håti, NTNU, Trondheim. Subdist takes the text file created using *ForceSpecAnalys* as an input. The program is used to plot forces vs. loading rates, divide the plot into sub distributions, create a histogram for each sub distribution, and fit Bell-Evans distribution of lifetimes to each histogram. From these fits the parametric values for f^* were used to plot

26

the dynamic strength spectrum. The program enables full control of sub distribution splitting, as well as setting the number of bins for each histogram. And this program enables the user to choose the ideal histogram amongst the created histograms. As long as the f^* values are independent of the number of bins, the sub distributions contain sufficient amounts of data points since the resulting dynamic strength spectrum will give bin-independent parametric values for x_β and k^0. If on the other hand the f^* values change with changing number of bins, as shown in Figure (4.2), the force-loading rate plot has to be split into larger sub distributions such that they contain more data points. The analytical procedure carried out using SubDist can be described in steps:

Upload text file containing analyzed data points from *ForceSpecAnalys* and spilt these points into a chosen number of sub distributions

1. Plot histograms for each sub distribution and fit Bell-Evans distribution of lifetimes to each histogram

2. Regulate the number of bins for each histogram to examine if the parametric value for f^* is bin dependent

3. Select the sub distributions with bin independent f^* values and plot the dynamic strength spectrum. A good fit for the dynamic strength spectrum would give small Δx_β and Δk^0 values and $R^2 \sim 1$.

4. If the dynamic strength spectrum yields poor values for R^2, Δx_β and/or Δk^0, divide into fewer sub distributions and repeat the procedure.

4.7.3 Life time Analysis

The script, ForceLifetimeFit, used to carry out the lifetime analysis described previously, was also kindly developed by Professor Bjørn T. Stokke.

A noteworthy difference from the Bell-Evans analytical procedure is that the created histograms are not used as data points for theoretical fits i.e. fits of (4.17), but instead used to determine analytical lifetimes for corresponding forces and loading rates. Therefore, by splitting the data into numerous sub distributions with a high amount of histogram bins, would yield higher amount of data points for the analytically determined lifetimes. This is desirable since the lifetime vs. force plot would contain an optimal amount of observations, and the fit of the theoretical lifetime expression (4.20) would provide good estimates for the parametric values of x_β, k^0 and ΔG. The script provides analytical determinations of the force dependent lifetimes, as well as a fit of the theoretical expression, including estimates for the parametric values of x_β and k^0 for all three possibilities of υ, and ΔG for υ=1, υ =1/2 and $\upsilon = 2/3$.

5. Results

In the First part of study, interactions between mucin immobilized onto the mica surfaces and different alginates onto the AFM tips were investigated. All seven complexes were shown to interact, however, due to insufficient data for the 0.01 mg/ml of mucin and 0.02 mg/ml of Mid-G alginate complex, the dataset for this complex is not presented. For all complexes, the Bell-Evans analysis and obtained results from the lifetime analysis are presented. The lifetime values with corresponding force magnitudes were determined by using the force measurement with corresponding loading rates. These were divided into 50 sub distributions (upper limit of the *ForceLifetimesFit* script), and plotted as histograms.

Moreover, together with the lifetime analysis, a regression with fixed x_β values is obtained for force measurements with corresponding loading rates is included (the same force vs loading rate plot as shown in the Bell-Evans part). This regression was performed with fixed x_β values from the corresponding lifetime analysis, to determine the compliance between the methods. Error estimates are not included for the lifetime analysis since they are negligibly small compared to the obtained parametric values, due to satisfying regression coefficients.

5.1 Mucin and High-G Alginate

Data were collected in liquid cell (aqueous 25 mM HEPES buffer, 150 mM NaCl, pH 6.9) for different low concentrations of Mucin and high-G alginate.

5.1.1 0.01 mg/ml Mucin and 0.02 mg/ml High-G Alginate

Very first data collection was for lowest concentrations of both mucin and High-G alginate as it is showed in table (4.3) in previous chapter, and 559 data points were obtained.

Data collected from interactions between 0.01 mg/ml Mucin and 0.02 mg/ml high-G alginate (559 data points in total), were divided into fifty distributions for life time analysis and into four sub-distributions for Bell Evans analysis. Parametric estimates from the three different distributions for three different v, as well as estimates obtained from the dynamic strength spectrum are presented in Table (5.1).
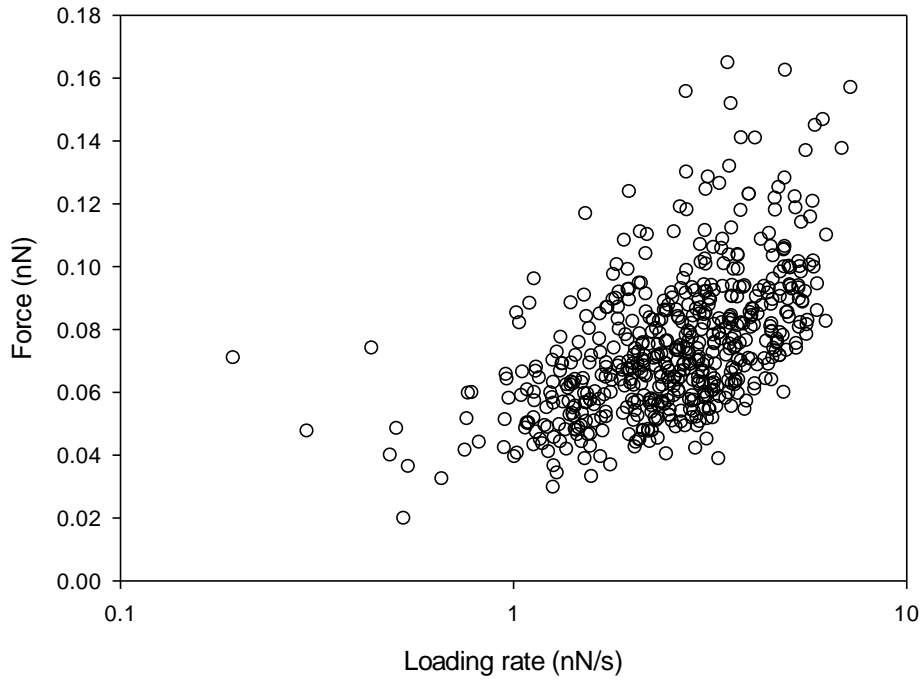
Figure 5.1: The force (nN) vs. loading rate (nN/s) plot for 0.01 mg/ml Mucin and 0.02 mg/ml high-G alginate consists of 559 data points.

Table 5.1: Here, the estimated parametric values obtained from Lifetime analysis for different υ parameters. The last row represent the fit related to Bell Evans analysis.

Mucin and HG Alginate	$\tau\ (s)$	$x_\beta\ (nm)$	ΔG
$\upsilon = 1/2$	0.056	0.126	42.132
$\upsilon = 2/3$	0.056	0.126	33.126
$\upsilon = 1$	0.056	0.126	---
	0.216	0.174	---

5.1.2 0.03 mg/ml Mucin and 0.06 mg/ml High-G Alginate

Data collected from interactions between 0.03 mg/ml Mucin and 0.06 mg/ml high-G alginate 417 data points in total, were divided into fifty distributions for life time analysis and into Three sub-distributions for Bell Evans analysis. Parametric estimates from the three different distributions for three different υ, as well as estimates obtained from the dynamic strength spectrum are presented in Table (5.2).
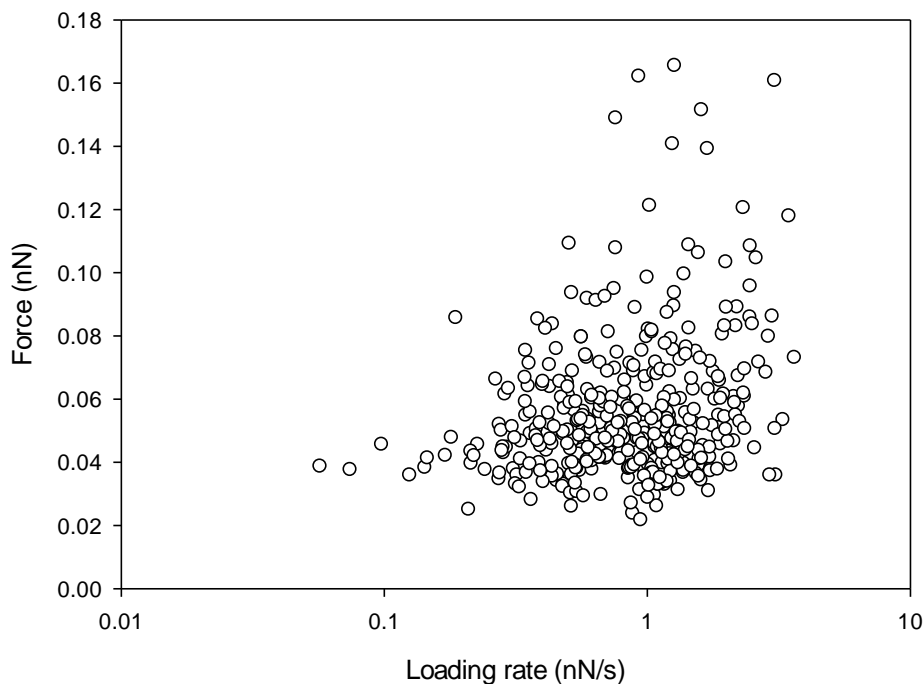
30

Figure 5.2: The force vs. loading rate plot for 0.03 mg/ml Mucin and 0.06 mg/ml high-G alginate consists of 417 data points.

Table 5.2: Here, the estimated parametric values obtained from Lifetime analysis for different v parameters. The last row represents the fit related to Bell Evans analysis.

Mucin and HG Alginate	τ (s)	x_β (nm)	ΔG
$v = 1/2$	0.191	0.241	42.132
$v = 2/3$	0.187	0.235	33.126
$v = 1$	0.187	0.235	---
	50	0.71	---

5.1.3 0.05 mg/ml Mucin and 0.1 mg/ml High-G Alginate

Data collected from interactions between 0.03 mg/ml Mucin and 0.06 mg/ml high-G alginate 946 data points in total, were divided into fifty distributions for life time analysis and into Three sub-distributions for Bell Evans analysis. Parametric estimates from the five different distributions for three different v, as well as estimates obtained from the dynamic strength spectrum are presented in Table (5.3).
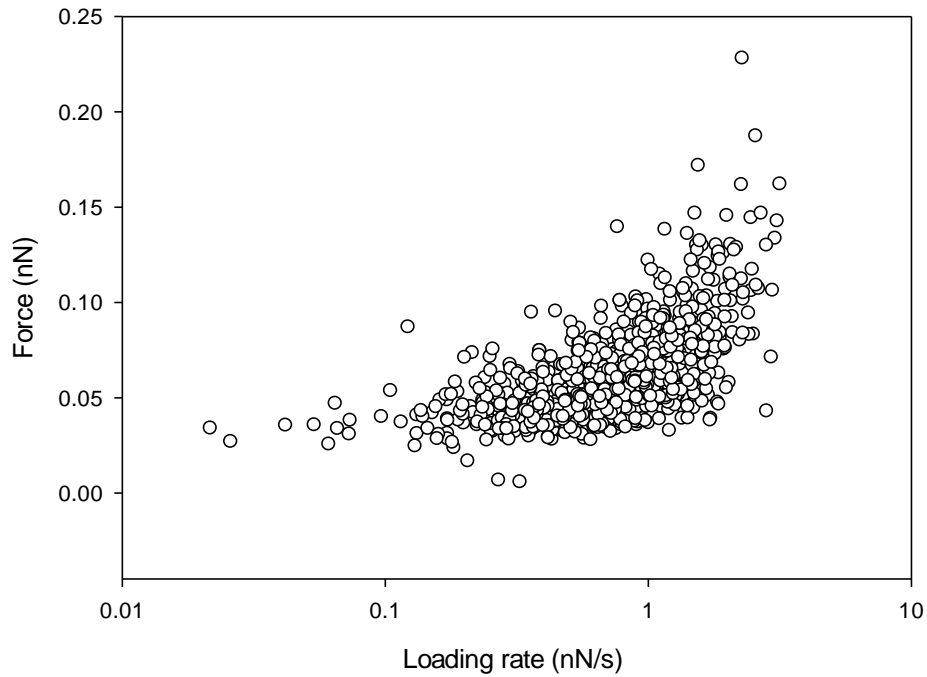
Figure 5.3: The force (nN) vs. loading rate (nN/s) plot for 0.05 mg/ml Mucin and 0.1 mg/ml high-G alginate consists of 946 data points.

Table 5.3: Here, the estimated parametric values obtained from Lifetime analysis for different v parameters. The last row represents the fit related to Bell Evans analysis.

Mucin and HG Alginate	$\tau\ (s)$	$x_\beta\ (nm)$	ΔG
$v = 1/2$	0.191	0.241	0.049
$v = 2/3$	0.167	0.137	50.959
$v = 1$	0.168	0.137	---
	1.369	0.28	---

5.1.4 0.03 mg/ml Mucin and 0.06 mg/ml Mid-G Alginate

Data collected from interactions between 0.03 mg/ml Mucin and 0.06 mg/ml Mid-G alginate, 190 data points in total, were divided into fifty distributions for life time analysis and into three sub-distributions for Bell Evans analysis. Parametric estimates from the three different distributions for three different v, as well as estimates obtained from the dynamic strength spectrum are presented in Table (5.4).

Figure 5.4: The force vs. loading rate plot for 0.03 mg/ml Mucin and 0.06 mg/ml Mid-G alginate consists of 190 data points.

Table 5.4: Here, the estimated parametric values obtained from Lifetime analysis for different v parameters. The last row represents the fit related to Bell Evans analysis.

Mucin and MG Alginate	$\tau\ (s)$	$x_\beta\ (nm)$	ΔG
$v = 1/2$	0.084	0.257	0.024
$v = 2/3$	0.069	0.214	0.022
$v = 1$	0.069	0.214	---
	0.16	0.18	---

5.1.5 0.05 mg/ml Mucin and 0.1 mg/ml Mid-G Alginate

Data collected from interactions between 0.05 mg/ml Mucin and 0.1 mg/ml Mid-G alginate, 459 data points in total, were divided into fifty distributions for life time analysis and into four sub-distributions for Bell Evans analysis. Parametric estimates from the three different distributions for three different v, as well as estimates obtained from the dynamic strength spectrum are presented in Table (5.5).
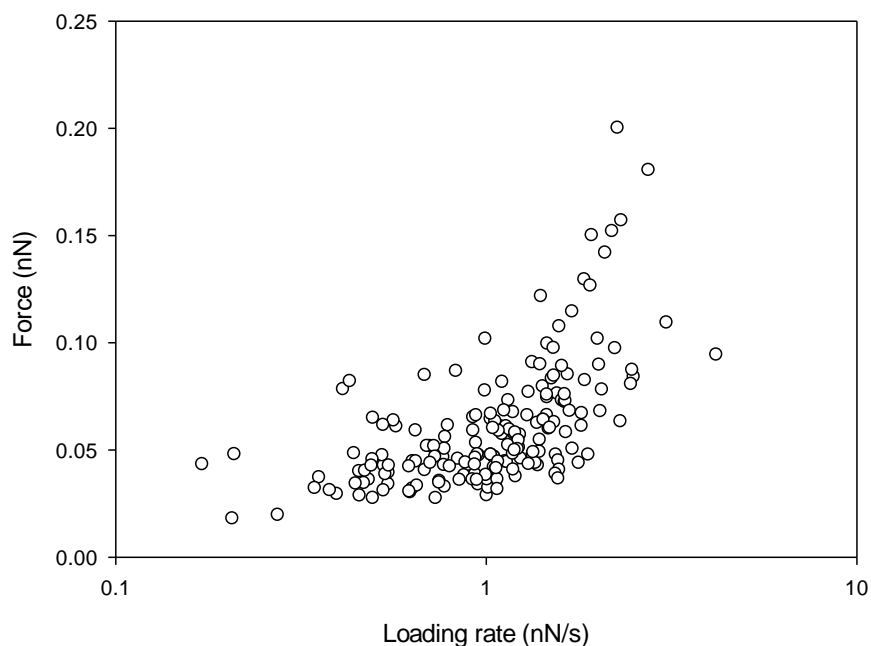
Figure 5.5: The force (nN) vs. loading rate (nN/s) plot for 0.05 mg/ml Mucin and 0.1 mg/ml Mid-G alginate consists of 459 data points.

Table 5.5: Here, the estimated parametric values obtained from Lifetime analysis for different v parameters. The last row represents the fit related to Bell Evans analysis.

Mucin and MG Alginate	τ (s)	x_β (nm)	ΔG
$v = 1/2$	0.040	0.185	0.029
$v = 2/3$	0.039	0.176	0.024
$v = 1$	0.039	0.176	---
	0.074	0.119	---

5.1.6 0.05 mg/ml Mucin and 0.1 mg/ml Pseudomonas Alginate

Data collected from interactions between 0.05 mg/ml Mucin and 0.1 mg/ml pseudomonas alginate, 555 data points in total, were divided into fifty distributions for life time analysis and into four sub-distributions for Bell Evans analysis. Parametric estimates from the three different distributions for three different v, as well as estimates obtained from the dynamic strength spectrum are presented in Table (5.6).
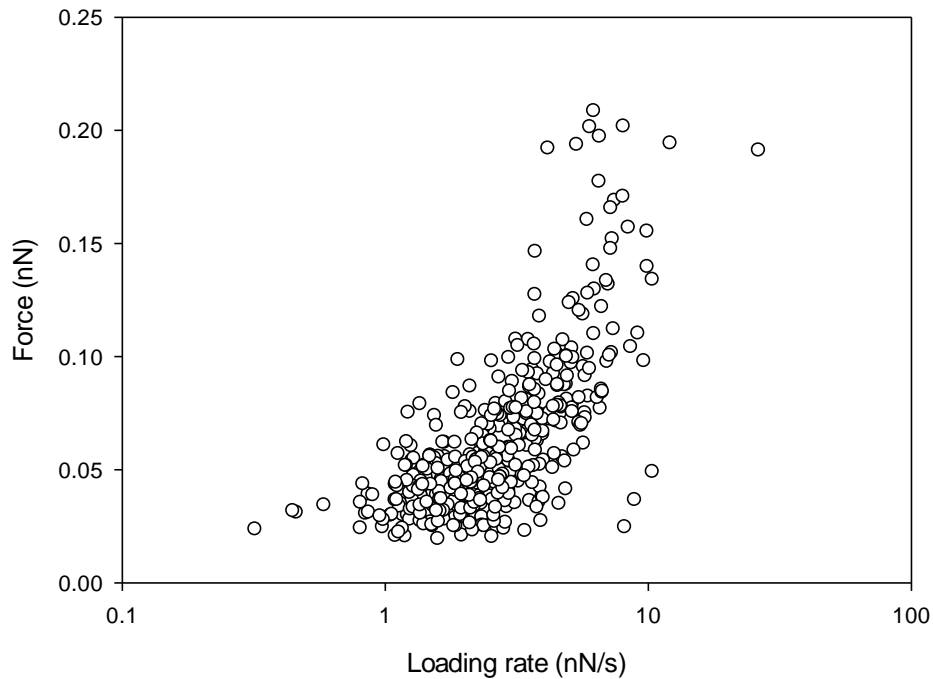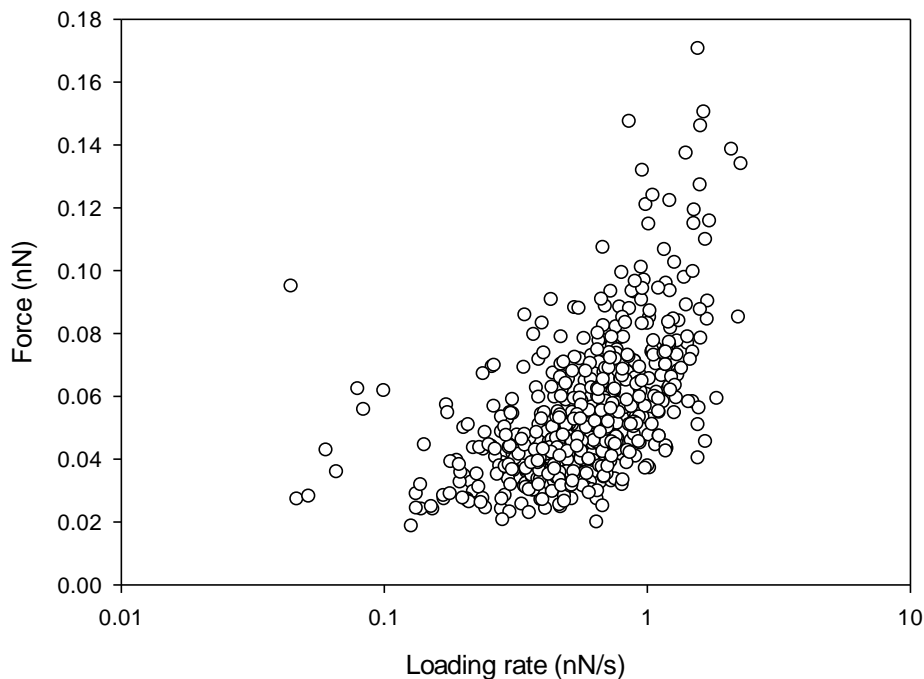
34

Figure 5.6: The force (nN) vs. loading rate (nN/s) plot for 0.05 mg/ml Mucin and 0.1 mg/ml pseudomonas alginate consists of 555 data points.

Table 5.6: Here, the estimated parametric values obtained from Lifetime analysis for different v parameters. The last row represents the fit related to Bell Evans analysis.

Mucin and Psu. Alginate	$\tau\ (s)$	$x_\beta\ (nm)$	ΔG
$v = 1/2$	0.18781224	0.16810068	21.169272
$v = 2/3$	0.18780475	0.16809054	17.527826
$v = 1$	0.18780475	0.16809054	---
	0.4	0.179	---

Amongst these complexes the 0.05 mg/ml mucin and 0.1 mg/ml Mid-G alginate is chosen for more investigation about gelation properties in presence of Ca^{2+}. Mid-G alginate is chosen because its reduced gelation in comparison with High-G alginate and the concentration is chosen due to the number of data points.

5.1.7 Mucin and High-G Alginate

In this part all the data points from force jumps of single molecule interactions of mucin-High-G alginates are combined together to give more data points for having more reliable results.

Data collected from interactions between different concentrations of mucin and different concentration of High-G alginate, 955 data points in total, were divided into fifty distributions for life time analysis and into seven sub-distributions for Bell Evans analysis. Parametric estimates from the three different distributions for three

different v, as well as estimates obtained from the dynamic strength spectrum are presented in Table (5.7).

Figure 5.7: The force (nN) vs. loading rate (nN/s) plot for three Mucin and High-G alginate consists of 955 data points.

Table 5.7: Here, the estimated parametric values obtained from Lifetime analysis for different v parameters. The last row represents the fit related to Bell Evans analysis.

Mucin and HG Alginate	τ (s)	x_β (nm)	ΔG
$v = 1/2$	0.181	0.174	22.410
$v = 2/3$	0.181	0.174	25.79
$v = 1$	0.181	0.174	---
	1.29	0.29	---

36
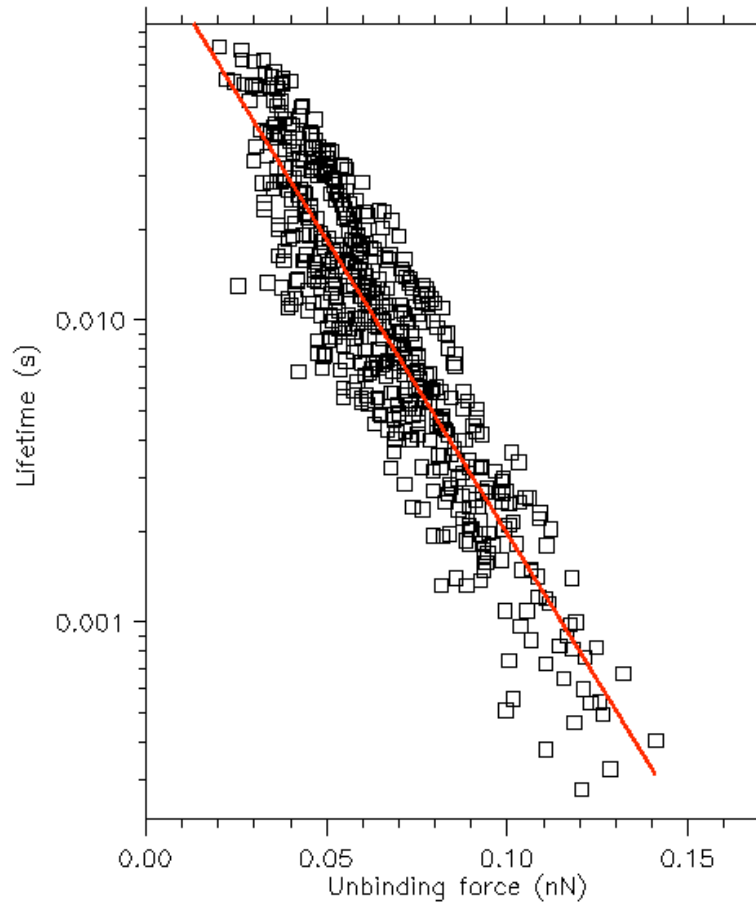
Figure 5.8: illustrate the lifetime (s) vs. unbinding force (nN) for $v = 1$.

5.1.8 Mucin and Mid-G Alginate

In this part all the data points from force jumps of single molecule interactions of mucin-Mid-G alginates are combined together to give more data points for having more reliable results.

Data collected from interactions between different concentrations of mucin and different concentration of Mid-G alginate, 649 data points in total, were divided into fifty distributions for life time analysis and into four sub-distributions for Bell Evans analysis. Parametric estimates from the three different distributions for three different v, as well as estimates obtained from the dynamic strength spectrum are presented in Table (5.8).
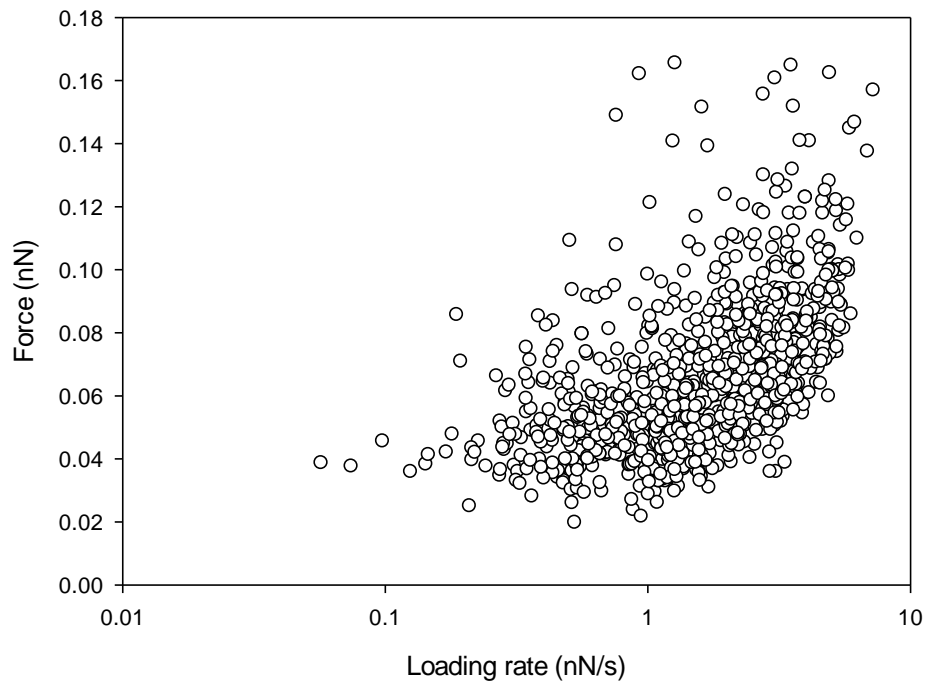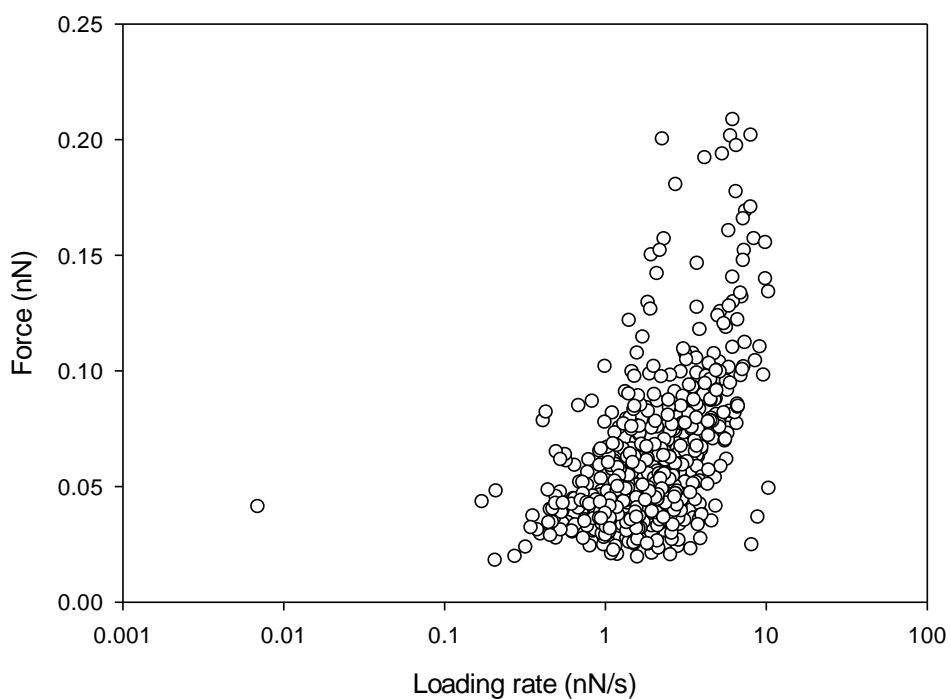
Figure 5.9: The force (nN) vs. loading rate (nN/s) plot for two Mucin and Mid-G alginate consists of 649 data points.

Table 5.8: Here, the estimated parametric values obtained from Lifetime analysis for different v parameters. The last row represents the fit related to Bell Evans analysis.

Mucin and MG Alginate	$\tau \ (s)$	$x_\beta \ (nm)$	ΔG
$v = 1/2$	0.20	0.070	22.410
$v = 2/3$	0.193	0.068	25.79
$v = 1$	0.19	0.068	---
	0.12	0.16	---
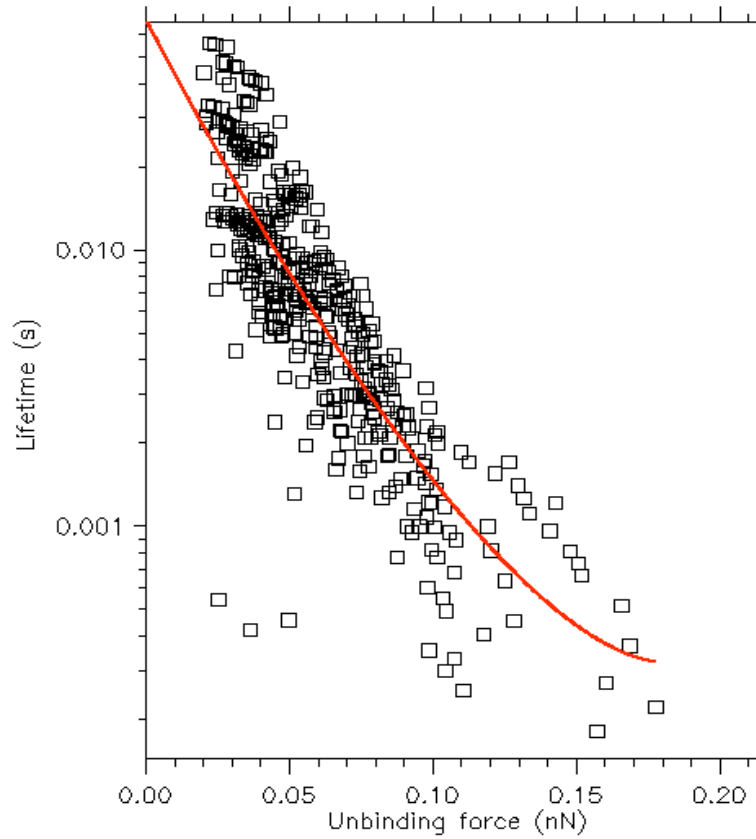
Figure 5.10: illustrate the lifetime (s) vs. unbinding force (nN) for $v = 1$.

5.1.9 0.05 mg/ml Mucin and 0.1 mg/ml Mid-G Alginate

In this part the data were collected first in the liquid cell (aqueous 25 mM HEPES buffer, 150 mM NaCl, pH 6.9) and for the second one liquid cell was (aqueous 10mM EGTA in 25 mM HEPES buffer, 150 mM NaCl, pH 6.9), third one was (aqueous 1mM Ca^{2+} in 25 mM HEPES buffer, 150 mM NaCl, pH 6.9), fourth one was (aqueous 1mM Ca^{2+} and 10mM EGTA in 25 mM HEPES buffer, 150 mM NaCl, pH 6.9) at room temperature.

Table 5.9: Here, the estimated parametric values obtained from Lifetime analysis for different v parameters. The last row represents the fit related to Bell Evans analysis. (Aqueous 25 mM HEPES buffer, 150 mM NaCl, pH 6.9)

Mucin and MG Alginate	$\tau\ (s)$	$x_\beta\ (nm)$	ΔG
$v = 1/2$	0.088046331	0.11979202	22.165540
$v = 2/3$	0.088038924	0.11977282	38.174098
$v = 1$	0.088038924	0.11977282	---
	0.613	0.263	---

Table 5.10: Here, the estimated parametric values obtained from Lifetime analysis for different v parameters. The last row represents the fit related to Bell Evans analysis. (Aqueous 10mM EGTA in 25 mM HEPES buffer, 150 mM NaCl, pH 6.9)

Mucin and MG Alginate	τ (s)	x_β (nm)	ΔG
$v = 1/2$	0.16700545	0.32657147	0.027867796
$v = 2/3$	0.12608270	0.26628391	0.026467952
$v = 1$	0.12608270	0.26628391	---
	0.22	1.35	---

Table 5.11 Here, the estimated parametric values obtained from Lifetime analysis for different v parameters. The last row represents the fit related to Bell Evans analysis. (Aqueous 1mM Ca^{2+} in 25 mM HEPES buffer, 150 mM NaCl, pH 6.9)

Mucin and MG Alginate	τ (s)	x_β (nm)	ΔG
$v = 1/2$	0.15290978	0.15612764	0.45938508
$v = 2/3$	0.15308870	0.15656159	0.25085707
$v = 1$	0.15308870	0.15656159	---
	4.16	0.53	---

Table 5.12: Here, the estimated parametric values obtained from Lifetime analysis for different v parameters. The last row represents the fit related to Bell Evans analysis. (Aqueous 1mM Ca^{2+} and 10mM EGTA in 25 mM HEPES buffer, 150 mM NaCl, pH 6.9)

Mucin and MG Alginate	τ (s)	x_β (nm)	ΔG
$v = 1/2$	0.11446896	0.19206207	5.4886420
$v = 2/3$	0.11439625	0.19189734	12.238312
$v = 1$	0.11439625	0.19189734	---
	50	0.76	---

Table 5.13: the estimated parametric values obtained from Lifetime analysis for different $v = 1$.

Solution	τ (s)	x_β (nm)
HEPES BUFFER	0.088	0.11
10 mM EGTA BUFFER	0.126	0.26
1mM Ca^{2+} BUFFER	0.153	0.17
10 mM EGTA + 1mM Ca^{2+} BUFFER	0.114	0.23

Table 5.14: the estimated parametric values obtained from Bell Evans analysis.

Solution	τ (s)	x_β (nm)
HEPES BUFFER	0.088	0.11
10 mM EGTA BUFFER	0.126	0.26
1mM Ca^{2+} BUFFER	0.153	0.17
10 mM EGTA + 1mM Ca^{2+} BUFFER	0.114	0.23

6. Discussion

6.1 Experimental Challenges

6.1.1 Mucin-Alginate measurements

In total seven studied complexes in the first part and one complex in the second part, four involved Mid-G alginate, three involved High-G alginate and one pseudomonas alginate. From the different force vs. loading rate plots presented in the previous chapter, it is clear that interactions between the studied 0.01 mg/ml mucind-0.02 mg/ml Mig-G alginate show lack of data points for loading rate values compared to plots for 0.05 mg/ml mucin-0.1 mg/ml pseudomonas alginate and 0.05 mg/ml mucin-0.1 High-G alginate interactions. Interactions for the mucin-Mid-G alginate systems with concentration below 0.03 mg/ml mucin-0.06 mg/ml Mid-G alginate were seldom observed and is a direct consequence of experimental difficulties. This is the main reason that in this study the chosen concentration for second part of experiment is higher concentrations both for mucin and alginate but due to gelation properties of alginate the chosen alginate is Mid-G alginate to eliminate the gelation in comparison with High-G alginate during measurements to get the best visible gelation due to having Ca^{2+} in the buffer solution.

6.2 Analytical Procedure

6.2.1 Analytical Challenges

When the AFM is used to study single-molecule unbinding events, multiple interactions are often present to some extent. This is evident from force curves containing unrealistically high force measurements. Preparation of samples to get enough low concentrations, as well as the collection of force jumps, should therefore be carried out with great care and persistence.

During data collection it is not possible to make sure that all of the selected interactions are pure single molecule interactions. Multiple interactions are to some extent collected, but an effect on the end result is not necessarily visible.

Testing the importance of high force measurements can be performed using statistical procedures, such as applying a weighting function to the dataset when further analysis and regressions are carried out. The weighting function can be set to gradually lower the importance of measurements towards the high force region For the Bell-Evans method, the effect of a weighting function was tested for fits to each histogram, while holding the number of histogram bins constant. Although parametric values for x_β and k^0 were somewhat affected the parametric values for f^* were more or less unchanged. The dynamic strength spectra, in the case of the seven analyzed datasets, were thus concluded to be virtually insensitive to multiple interactions. Nevertheless, it has to be borne in mind that for even higher amounts of multiple interactions, the dynamic strength spectra will eventually be affected. The effect of a weighting function was more obvious when applied to the fit of (3.18) on the analytically

determined lifetimes. The parametric values of x_β, k^0 and ΔG were somewhat affected with and without different weighting functions. Since interactions in the low force region are judged to be trust worthier as single-molecule interactions, and the probability of counting multiple interaction increase with force, the datasets were analyzed with the weighting function:

$$W = \frac{1}{force^2}$$

6.2.2 Bell-Evans routine vs. Lifetime analysis

The collected force jumps for all studied mucin-alginate interactions (except for 0.01 mg/ml mucin-0.02 Mid-G alginate due to lack of force measurements) were further analyzed with the two different analytical routines described previously. As previously mentioned, in the case of the Bell-Evans analytical procedure, the sub distributions containing sufficient amounts of data points yielding *bininsensitive* parametric values for f^*, were applied for the calculation of the dynamic strength spectrum. Through plentiful trial error attempts, different combinations of number of sub distributions, and number of bins for each sub distribution histogram, were tested for all the analyzed datasets. A congruent conclusion for all mucin-alginate datasets states as follows: Even though some sub distributions provided bin-insensitive f^* values, the datasets had to be divided into too large sub distributions in order to obtain such values, yielding poor regression goodness for the fits of (3.16) to the f^* and $< r_f >$ leading to poor estimates of x_β and k^0 from the dynamic strength spectra. The dynamic strength spectra, although they were concluded to be more or less insensitive to multiple interactions, are however, sensitive to the choice of sub distributions and number of histogram bins within each sub distribution. For each sub distributions to provide completely bin-insensitive f^* values (for a dataset with a majority of single-molecule interactions), approximately 300-400 data points were needed. Moreover, deviations between x_β and k^0 values from each sub distribution and the dynamic strength spectrum within the same datasets, are also evidence of poor parametric estimates obtained from the spectrum. Note, however, that although the dynamic strength spectra are less trustworthy due to strong bin sensitivity, the fit of (3.17) to individual sub distribution histograms often provide trustworthy parametric values for x_β and k^0 and f^*, again depending on the number of data points and the relative count of multiple interactions.

The lifetime analysis routine is in many ways less challenging to implement, especially given the fact that only three fits ($v = 1, v = 1/2$ and $v = 2/3$) are needed to determine parametric estimates for x_β and k^0 and ΔG, and to validate the energy landscape assumptions. Since all analytically determined lifetimes are used to calculate these estimates (not divided into sub distributions), this procedure is more robust and provides better fit goodness than what could be said for the dynamic strength spectra. Thus, this routine is more advantageous for datasets with fewer observations. Additionally, an estimate for the Gibbs free energy ΔG can be found from this procedure, which is not possible with the Bell-Evans method.

Ideally, the analytical routines should provide congruent parametric estimates for x_β and k^0. Since the dynamic strength spectra do not provide trustworthy parametric

values, however, a direct comparison between the obtained values for x_β and k^0 from the two methods cannot be performed. A different approach to compare the methods was therefore implemented: By treating all the collected forces in the force vs. loading rate plot as f^* values, a dynamic strength spectrum (with infinitely narrow sub distributions) was obtained by fitting (3.16) to all measured forces with corresponding loading rates. To more clearly see the correspondence between the parametric estimates from this method and the lifetime analysis routine, x_β obtained from the lifetime analysis with $\upsilon = 1$ (Bell Evans barriers/wells), was held constant when the regression to the force vs. loading rate plot was carried out. This way, a comparison between parametric values of τ^0 from the two methods could roughly determine the compliance between the methods.

The dependence of high number of observations to obtain good theoretical fits and thus good parametric estimates, makes dynamic force spectroscopy a challenging technique, limited to molecule-pairs that are able to provide plentiful experimental observations.

6.2.3 Energy landscape assumptions

The parametric values obtained for x_β and τ^0 show significant should show variations between the different fits of υ for almost all the complexes. Therefore, the underlying nature of the energy barriers must be accounted for. But due to lack of data points it cannot be seen in some cases.

6.4 Biological interpretation

6.4.1 Mucin and Alginate in HEPES buffer

According to obtained parameters at higher physical displacement of the molecules mucin and HighG is required to dissociate the complex than what is expected for the mucin-midG complex, which is reflected by the higher parametric value of x_β for the mucin-highG. This may be due to an extended subsite for the mucin-highG complex, and supports the fact that mucin is thought to have a higher affinity to G-monomers than to M-monomers.

No substantial difference between the lifetimes. A conclusion on the physical meaning of it, other than the fact that it indicates that the complexes are formed and dissociate with the same time duration, is hard to draw.

6.4.2 Mucin and Alginate in different buffers

As said by the data that is obtained in these study mucin-alginate interactions in HEPES buffer shows high x_β and τ in this case we might have some calcium in our inviroments. By presence of Ca^{2+} in the solution it will sits between mucin and Mid-G alginates and it does not let them to interact properly. In such this situation we used

the 10mM EGTA buffer to skip the Ca^{2+}, influence on interactions. By adding 10mM EGTA it is expected to get highest x_β and τ because there is no more Ca^{2+}, mucin and Mid-G alginate can make stronger bonds. In the next step data collection was done in 1mM Ca^{2+} buffer, we expect to get lowest x_β and τ due to presence of Ca^{2+} the mucin and Mid-G alginate will make weaker bonds so the bond rupture will be easier. The last step is having looking the competition between EGTA and Ca^{2+} in this case it seems that Mid-G alginate is more likely bonds to EGTA not Ca^{2+} that's why the x_β and τ are in the medium stage in comparison with two previous cases.

The parameters, which are gotten from Lifetime analysis and Bell Evans analysis, are in common track. They are not identical but they are siting in same order. The parameters which are gotten from Bell Evans for parameter τ is not really reliable due to lack of data points.

7. Concolusion

Force Robot JPK 300 was used to investigate the interactions between mucin and different alginate in different environments to give the better understanding details of molecular interaction between alginate and mucin. It was expected that interactions are dependent on structural properties of the biomacromolecules and co-factors existing in solution. Parameters in the energy landscapes of the interactions like the separation distance to barrier and lifetime are expected to reflect such differences.

As it was discussed according to obtained parameters at higher physical displacement of the molecules mucin and HighG and mucin-midG complex it was obtained that parametric value of x_β for the mucin-highG is higher so it can be seen mucin and High-G alginates makes stronger bonds that for their rupture we need higher force.

During this study we obviously understood the influence of presence of Ca^{2+} as we have more Ca^{2+} we would get lower displacement factor it means that when mucin face Ca^{2+} as a cofactor in between its interaction with alginate it cannot bonds between mucin and alginate will be weaker because of a presence of a bridge in between.

The parameters which was given by Lifetime analysis and Bell Evans analysis were somehow far from each other it can be due to lack of sufficient number of data points. For having more data points it is better to try different speeds as well.

8.Bibliography

[1] Welsh MJ, Ramsey BW, Accurso FJ, Cutting GR. In: Scriver CR, Beaudet AL, Valle D, Sly WS, editors. The metabolic and molecular bases of inherited disease. New York: McGraw Hill; 2001. pp. 521–588

[2] Davis PB. Am J Respir Crit. Cystic fibrosis since 1938. Care Med 2005;173:475–482

[3] Samuel M Moskowitz, MD, James F Chmiel, MD, Darci L Sternen, MS, CGC, Edith Cheng, MS, MD, and Garry R Cutting, MD CFTR-Related Disorders.. Bookshelf ID: NBK1250PMID: 20301428. Initial Posting: March 26, 2001; Last Update: February 19, 2008

[4] T B May, D Shinabarger, R Maharaj, J Kato, L Chu, J D DeVault, S Roychoudhury, N A Zielinski, A Berry and R K Rothmel Clin Alginate synthesis by Pseudomonas aeruginosa: a key pathogenic factor in chronic pulmonary infections of cystic fibrosis patients.. Microbiol. Rev. 1991, 4(2):191. DOI: 10.1128/CMR.4.2.191

[5] J R Govan and V Deretic .Microbial pathogenesis in cystic fibrosis: mucoid Pseudomonas aeruginosa and Burkholderia cepacia.. Microbiol. Mol. Biol. Rev. September 1996 vol. 60 no. 3 539-574

[6] Marit Sletmoen,a Gjertrud Maurstad,a Catherine Taylor Nordgard, b Kurt Ingar Dragetb and Bjørn Torger Stokke . Oligoguluronate induced competitive displacement of mucin–alginate interactions: relevance for mucolytic function.

[7] Deborah M. Ramsey, Daniel J. Wozniak. Understanding the control of Pseudomonas aeruginosa alginate synthesis and the prospects for management of chronic infections in cystic fibrosis. Molecular Microbiology Volume 56, Issue 2, pages 309–322, April 2005

[8] Nikolaos A. Peppas .Hydrogels in medicine and pharmacy.. fundamentals, vol. 1. Boca Raton, FL: CRC Press, 1986.

[9] Crooks CA, Dougles JA, Broughton RL, Sefton MV. A sub- merged jet process for the microencapsulation of mammalian cells in a HEMA-MMA copolymer.. J Biomed Mater Res 1990; 24:1241—62

[10] Jen AC, Wake MC, Mikos AG. Review: hydrogels for cell immobilization. Biotechnol Bioeng 1996;50:357—64

[11] Olav Smidsrød, Prof. Dr. Gudmund Skjåk Bræk. Alginate as immobilization matirix for cells. TIBTECH 1990;8:71—8.

[12] Dr. Kurt Ingar Draget, Prof. Dr. Olav Smidsrød, Prof. Dr. Gudmund SkjAåk Bræk. Alginates from Algae.

[13] Tsau-Yen Lin and W. Z Hassid. Pathway of alginic acid synthesis in the marine brown alga, fucus gardneri silva.. Journal of Biological Chemistry, 241(22):5284–

5297, November 1966.

[14] MartinsenA, Olav Smidsrød. Gudmund Skjåk Bræk .Alginate as immobilzation material. I. Correlation between chemical and physical prop- erties of alginate gel beads.. Biotechnol Bioeng 1989;33:79—89

[15] Arne Haug, Bjørn Larsen, and Olav Smidsrød. Uronic acid sequence in alginate from different sources. Carbohydrate Research, 32(2):217–225, February 1974.

[16] Morris E R Grant G T. Biological interactions between polysaccharides and divalent cations:the eggbox model. FEBS Letters, 32(02), 1973.

[17] Inger Mari Nygård Vold, Kåre A. Kristiansen, and Bjørn E. Christensen. A study of the chain stiffness and extension of alginates, in vitro epimerized alginates, and Periodate-Oxidized alginates using Size-Exclusion chromatography combined with light scattering and viscosity detectors.. Biomacromolecules, 7(7):2136–2146, 2006.

[18] Helga Ertesvåg, Svein Valla, and Gudmund Skjåk-Bræk. Enzymatic alginate modification.. In Bernd H. A. Rehm, editor, Alginates: Biology and Applications, volume 13 of Microbiology Monographs, pages 95–115. Springer Berlin / Heidelberg, 2009.

[19] Johnson, L., Ed. Structure and function of gastrointestinal mucus. Allen, A. In Physiology of the gastroenterology tract, 1st ed.;.; Raven Press: New York, 1981; pp 617-39.

[20] Matsui, H., Randell, S.H., Peretti, S.W., Davis, C.W., and Bouche. Coordinated clearance of periciliary liquid and mucus from air- way surfaces. r, R.C. 1998. J. Clin. Invest. 102:1125–1131.

[21] Michael R. Knowles and Richard C. Boucher J. Clin. Mucus clearance as a primary innate defense mechanism for mammalian airways
. Invest. 109:571–577 (2002). DOI:10.1172/JCI200215217.

[22] Bhaskar, D. H. Gong, R. Bansil, S. Pajevic, J. A. Hamilton, B. S. Turner and J. T. Profound increase in viscosity and aggregation of pig gastric mucin at low pH K. R. LaMont Am J Physiol Gastrointest Liver Physiol 261:G827-G832, 1991

[23] Immo Fiebrigab, Stephen E. Hardingb*, Arthur J. Roweed, Stefan C. Hymand & Stanley S. Davisa. Transmission electron microscopy studies on pig gastric mucin and its interactions with chitosan. Carbohydrate Polymers Volume 28, Issue 3, November 1995, Pages 239–244

[24] S. Girod, J-M. Zahm, C. Plotkowski, G. Beck, E. Puchelle Role of the physicochemical properties of mucus in the protection of the respiratory epithelium.. ERJ April 1, 1992 vol. 5 no. 4 477-487.

[25] Alos L, Lujan B, Castillo M, Nadal A, Carreras M, Caballero M, de Bolos C, Cardesa, Am J Surg Pathol. A Expression of membrane-bound mucins (MUC1 and

MUC4) and secreted mucins (MUC2, MUC5AC, MUC5B, MUC6 and MUC7) in mucoepidermoid carcinomas of salivary glands. 2005 Jun;29(6):806-13.

[26] Juan Perez-Vilar and Robert L. Hill. The Structure and Assembly of Secreted Mucins.. The Journal of Biological Chemistry, 274, 31751-31754

[27] F Ritort. Single-molecule experiments in biological physics methods and applications.. J. Phys.: Condens. Matter 18 (2006) R531–R583

[28] R. Derike Smiley and Gordon G. Hammes. Single molecule studies of enzyme mechanisms.. Chemical Reviews, 106(8):3080–3094, August 2006.

[29] Single molecule force spectroscopy in biology using the atomic force microscope. Progress in Biophysics and Molecular Biology, Volume 74, Issues 1–2, July–August 2000, Pages 37–61.

[30] Rief, M., Gautel, M., Oesterhelt, F., Fernandez, J. M. & Gaub, H. E. (1997) Science 276, 1109–1112.

[31] bonds O. K. Dudko, A. E. Filippov, J. Klafter, and M. Urbakh. Beyond the conventional description of dynamic force spectroscopy of adhesion.PNAS vol. 100 no. 20

[32] O. K. Dudko, A. E. Filippov, J. Klafter, and M. Urbakh. Beyond the conventional description of dynamic force spectroscopy of adhesion bonds.

[33] G. I. Bell. Models for the specific adhesion of cells to cells. Science,200(4342):618–627, May 1978.

[34] H.A. Kramers. Brownian motion in a field of force and the diffusion model of chemical reactions. Physica, 7(4):284–304, April 1940.

[35] Victor Muñoz. Conformational Dynamics and Ensembles in Protein Folding. Biophysics and Biomolecular Structure Vol. 36: 395-412 . 2007

[36] Cyrus Levinthal. Mossbauer Spectroscopy in Biological Systems Proceedings of a meeting held at Allerton House Monticello Illinois. University of Illinois Press, 1969.

[37] Barry Honig. Protein Folding: From the Levinthal Paradox to Structure Prediction. J. Mol. Biol. (1999) 293, 283±293

[38] ROBERT ZWANZIG. Two-state models of protein folding kinetics. Proc. Natl. Acad. Sci. USA. Vol. 94, pp. 148–150, January 1997. Biophysics

[39] Hairong Ma, Chaozhi Wan, Aiguo Wu, and Ahmed H Zewail. DNA folding and melting observed in real time redefine the energy landscape. Proceedings of the National Academy of Sciences, 104(3):712–716, January 2007.

[40] Evan Evans, PROBING THE RELATION BETWEEN FORCE LIFETIME AND CHEMISTRY IN SINGLEMOLECULAR BONDS. Biophys. Biomol. Struct. 2001. 30:105–28

[41] Evan Evans. Looking inside molecular bonds at biological interfaces with dynamic force spectroscopy. Biophysical Chemistry, 82(2–3):83–97, December 1999.

[42] Olga K. Dudko, Gerhard Hummer, and Attila Szabo. Intrinsic rates and activation free energies from Single-Molecule pulling experiments. Physical Review Letters, 96(10):108101, March 2006.

[43] Dr. Kurt Ingar Draget1, Prof. Dr. Olav Smidsrød2, Prof. Dr. Gudmund Skjåk-Bræk3. Alginates from Algae.

[44] Engel A, Lyubchenko Y, Müller D. Atomic force microscopy: a powerful tool to observe biomolecules at work.. Trends in Cell Biology [1999, 9(2):77-80]

[45] Cheryl R. Blanchard. Atomic Force Microscopy.. THE CHEMICAL EDUCATOR
December 1996, Volume 1, Issue 5, pp 1-8

[46] H J Kreuzer, S H Payne, and L Livadaru. Stretching a macromolecule in an atomic force microscope: statistical mechanical analysis. Biophys J. 2001 June; 80(6): 2505–2514.

[47] Wenke Zhang, Qiaobing Xu, Shan Zou, Hongbin Li, Weiqing Xu, and Xi Zhang. Molecule Force Spectroscopy on Bombyx mori Silk Fibroin by Atomic Force Microscopy Langmuir 2000, 16, 4305-4308Single.

[48] Hongbin Li a,b, Matthias Rief a, Filipp Oesterhelt a, Hermann E. Gaub a,), Xi Zhang b, Jiacong Shen Single-molecule force spectroscopy on polysaccharides by AFM – nanomechanical fingerprint of a-ž1,4/-linked polysaccharides.. Chemical Physics Letters 305 Ž1999. 197–201.